GENERAL ENGINEERING LABORATORY

SPACE POWER OPERATION

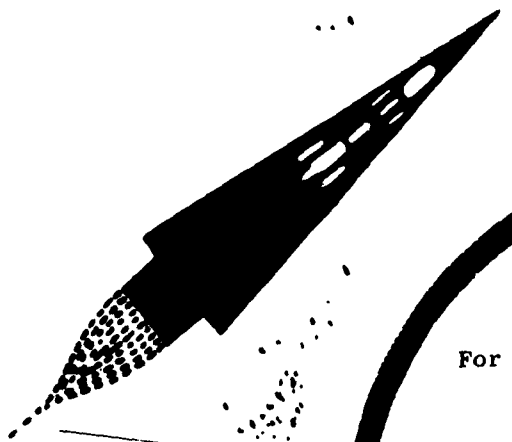

QUARTERLY REPORT NO. 1

For Period Ending February 9, 1962

VISCOSITY BEARING STABILITY INVESTIGATION

For

THE NATIONAL AERONAUTICS AND SPACE ADMINISTRATION

FLIGHT PROPULSION LABORATORY DEPARTMENT

GENERAL ELECTRIC

S P A C E P O W E R O P E R A T I O N

F I R S T Q U A R T E R L Y P R O J E C T S T A T U S R E P O R T

F E B R U A R Y 9 , 1 9 6 2

LOW VISCOSITY BEARING STABILITY INVESTIGATION
NATIONAL AERONAUTICS AND SPACE ADMINISTRATION

GENERAL ENGINEERING LABORATORY
AND
FLIGHT PROPULSION LABORATORY DEPARTMENT
GENERAL ELECTRIC COMPANY
CINCINNATI 15, OHIO

TABLE OF CONTENTS

TABLE OF CONTENTS (continued)

LIST OF FIGURES

I. SUMMARY

Bearing stability is one of the basic problems associated with high speed turbomachinery. It has become of even greater importance in space power systems presently under development by the requirement for long term unattended operation under zero g conditions of space flight, and low viscosity lubricants such as potassium at 1200°F.

The present program has been devised in answer to NASA P.R. G.S. 3526 of May 22, 1961. It consists of a combined analytical and experimental effort was begun to select and develop bearing configurations which promise stable operation up to the high speeds typical of space turbomachinery (35,000 rpm).

Main emphasis is placed on experimental investigations and evaluation. The experimental tool used is an especially designed high speed test rig, precision made for interchangeability of a large variety of bearing configurations and rotors. It is equipped with the most refined instrumentation to record rotor and bearing motions, as well as other parameters affecting bearing operation. The testing will be carried out at close to room temperature with lubricants which simulate the low viscosity and lubricity of liquid metals at operating temperatures.

The experimental program will be supplemented by analytical studies necessary to select the most promising bearing configurations, and to reduce test results to dimensionless parameters, permitting generalization of the information obtained.

It is anticipated that optimum bearing configurations meeting the conditions of stable, whirl free operation will be identified during the program.

The program is being carried out jointly by the Bearing and Lubricant Center of the General Engineering Laboratory in Schenectady, New York, and the Space Power Operation of F.P.L.D. in Cincinnati, Ohio. It thereby combines the most advanced analytical and experimental know-how in the field of high speed bearing development with extensive space power components, systems and development activities.

Using the bearing stiffness as a first approximative stability criterion analysis of different bearing types continued, to determine zero load radial bearing stiffnesses. The load carrying capacity at a minimum film thickness of 0.0005 inch of the bearing types considered has also been calculated.

Detailed design analysis of several test rig components has been completed. Considerable efforts have been spent to determine the natural frequencies of various shaft-bearing systems. Based on the results, a 1.25 inch diameter test shaft has been selected. The overall layout of the test rig has been completed and detailing of test rig components has been started.

Capacitance gauges have been checked out under simulated operating conditions including water and air.

II. INTRODUCTION

A. ORIGIN OF INVESTIGATION

The present trend toward higher operating speeds of rotating equipment has increased the need for knowledge of the dynamic behavior of such precision systems. It has been well recognized that bearings have a major influence upon the dynamic response of rotors. Fluid film instabilities or rotor vibrations arising from bearing phenomena may well provide major obstacles to achieving optimum rotor speeds and the compactness and low weight desired for many applications. It is the purpose of this program, therefore, to identify by analysis and experiment bearing configurations which promise the most stable shaft rotation when using liquid metals as bearing lubricants. Other considerations such as power loss, simplicity of manufacture and assembly, minimum film thickness will be evaluated in assessing the relative merits of the different bearing types. The program will therefore contribute to the establishment of design criteria for potassium lubricated bearings for operation at lubricant temperatures in the range of 800 to 1300°F and rotational speeds approaching 35,000 rpm.

B. PLAN OF INVESTIGATION

The main emphasis is placed on experimental investigation and evaluation. Analysis, however, will be employed as a guide to selecting the most promising bearing configurations and to correlating, interpreting and generalizing the test results obtained.

The overall program is divided into two phases. In Phase I, approximately eleven different bearing configurations are to be studied analytically and approximately nine selected for experimental evaluation. Simultaneously, a test facility is to be designed and manufactured for conducting such tests. The test facility permits control and measurement of the following important variables over the approximate ranges specified:

1. Shaft speed - 0 to 35,000 rpm.
2. Bearing load - Unidirectional 0 - 200 lbs.
   Rotating - 0 to maximum level as governed by maximum attainable speed, or by bearing load capacity.
3. Inlet lubricant pressure - 3 to 30 psi.
4. Inlet lubricant temperature - 100 to 160°F.
5. Clearances/inch diameter - 0.0016 to 0.004.
6. Bearing Length/diameter ratio - 0.75 to 1.5.
7. Shaft diameter - 1-1/4 inch.

All tests in Phase I will be conducted with distilled water as a lubricant. The stability behavior of the rotating shaft under the test conditions is to be measured with specially designed, non-contacting capacitance gauges.

In the analysis portion of the work conducted in Phase I, the major areas of investigations were defined in our proposal as:

1. Threshold speed of half-frequency whirl.
2. Amplitudes of synchronous whirl.
3. Rigid body critical speeds and amplitudes of vibrations.
4. Maximum film thickness and required lubricant flow.

Thus, in Phase I the anticipated behavior of a large number of different anti-whirl bearing configurations will be compared with experimental fact. This will indicate the extent to which the existing, simplified criteria of bearing stability is adequate; it will also provide the necessary confirmation for choosing the most promising bearing types for optimizing anti-whirl characteristics in Phase II.

In Phase II of this investigation, the three bearing configurations which demonstrate the most promising ability to suppress shaft whirl will be selected for further testing. A more detailed and refined analytical investigation will be made of the parameters that control shaft whirl, load carrying ability, friction torque and lubricant flow. The principal test lubricant in Phase II also will be distilled water. To verify the general validity of the information obtained, however, certain test points will be selected for testing with an additional test lubricant.

Upon conclusion of the tests, a comprehensive report will be issued in which the analysis and data will be correlated to form anti-whirl bearing design criteria.

C. TEST RIG DESIGN

1. Design Requirements

In establishing the design concept, the following requirements have been considered:

a. The bearings and shafts of the test rig should closely resemble the geometry of such elements in typical space power units.

b. In order to determine the effects of bearing clearance, bearing length/diameter ratio, and bearing geometry on the performance of dynamically loaded bearings, a large variety of bearing-shaft combinations must be evaluated.

c. The inherently small clearances of bearings lubricated with low viscosity fluids demand precision manufacturing methods for all vital parts, especially if interchangeability of bearings is provided.

d. The high rotational speeds of the test rotor require careful dynamic balancing in order to minimize the residual rotating load.

e. Although the tests are conducted at or near room temperature, the test rig material choice must minimize thermal expansion problems.

f. One of the important objectives of the experimental investigation is the study of shaft motion in dynamically loaded bearings in a zero g environment. It is, therefore, desirable to eliminate any restriction on shaft motion due to a thrust bearing or drive coupling.

g. Provision must be made for the reliable measurement of shaft locus, bearing torque, and shaft speed.

h. Both unidirectional and rotating loads must be accurately imposed on the bearings.

2. The Test Rig

A schematic of the originally proposed test rig is shown in Figure 1. The principle parts of the test rig are:

a. The test device.

b. High speed precision spindle with flexible quill shaft connection to the test rotor.

c. High speed two pole induction motor with a water cooled stator. Speed of the motor is controlled by variable frequency power supply.

The entire apparatus is hermetically sealed and can be tilted from the vertical to horizontal position with intermediate stops.

The drive arrangement must not influence the test conditions by introducing restraint on the rotor. A long, flexible quill shaft has been chosen as the drive connection to avoid these difficulties, as well as to eliminate a thrust bearing. The test rotor is free to adopt any mode of motion. The quill shaft is guided at close intervals in the hollow spindle shaft by Teflon bushings. The torque measurement of the bearing test rig is based on the angular deflection of the flexible quill shaft. This method requires no electrical connections to the rotating parts, nor does it complicate the bearing supports. A disk with 18 teeth is attached to the high speed precision spindle and is used to generate 18 pulses/revolution. A squaring amplifier shapes the pulse from the magnetic pick-up. Another pulse is generated by the other disk attached to the bearing test rotor. The series of pulses is fed into appropriate electronic equipment, which produces a DC voltage which is proportional to the torque. Between 3" and 20" torsional deflection of the quill shaft,

the torque meter records accurately the total friction and windage losses of the test rotor. The windage torque is relatively small compared to the bearing losses, (see Figures 10 and 11). Determination of test rotor speed is accomplished by using the 18 pulses per revolution from the serrated disk attached to the test rotor.

The occurrence of conical whirl at a speed lower than the threshold of translatory whirl is a function of the span length, the polar moment of inertia, the transverse moment of inertia, the rotor mass, and the bearing stiffness. Four basic variations of rotor mass and moment of inertia can be investigated with the 12.5 inch span test rig.

a. The plain shaft.

b. The shaft with one large flywheel.

c. The shaft with two small flywheels.

d. The shaft with two eccenters.

By exchanging the tubular casing of the test rig, the span length can be varied from 12.5 to 7.5 inches and three more variations of m, Ip and I_T are possible.

Unidirectional bearing loads are produced by two pneumatically-loaded partial arc (120°) bearings installed in the tubular test rig casing. The test rotors can be loaded slowly, step wise, or abruptly up to 400 lbs. total maximum load.

Rotating loads are achieved by two pairs of variable eccenters. By moving the eccentric disk of the variable eccenter counter to each other, the rotational loads can be varied as a function of shaft speed from zero to 1000 lbs. (see Figure 2). Angular gradients provided on shaft and eccenter disks allow the selection of the direction of the resultant eccenter forces with respect to the rotor.

With an eccentricity of 0.2 inch, the rotational load of one eccenter set easily exceeds 1000 lbs at 35,000 rpm, but can also easily decrease down to zero pound by shifting the eccenter halfs against each other. During bearing evaluations at high speeds, the maximum eccenter loads are not required, because the bearings load capacity is too small. At lower speeds, however, where the percentage of the rotating loads due to synchronoun rotor whirl and residual unbalance is small compared to bearing strength, maximum eccenter loads are necessary to obtain bearing eccentricity ratios > 0.~. In Figure 3, load capacity at various eccentricities of a cylindrical bearing 'L/D = 1.5) for two diameters, d = 1.25 inch and d = 1.5 inch, can be compared with the maximum rotating centrifugal loads obtainable with various unbalances.

III. STATUS OF INVESTIGATION

A. BEARING ANALYSIS

In the plan of investigation discussed earlier, four major areas of analytical investigation were outlined for selection of the nine preliminary test bearings. In each of these areas and for each bearing configuration, two items are of particular importance: (1) the position of the shaft center relative to a given load vector; and (2) the change in shaft center position for a given change in load, i.e. the film stiffness.

For bearings which are gravity loaded, the load assumes a fixed position relative to the bearing geometry. For the bearings under study in this program, however, the load vector position is completely arbitrary with respect to the bearing geometry. As a consequence, except for the few bearings possessing complete symmetry, the response of a typical non-symmetrical bearing depends upon both the magnitude and position of the load vector. A basic step in the analytical investigation, therefore, consists of determining the equilibrium shaft center position and the lubricant film stiffness for arbitrary position of the load vector.

Shaft displacement and radial fluid force vectors are not usually colinear. In the case of an infinitely long, full cylindrical bearing, for example, shaft displacement and load vectors are 90° apart in space. The component of the force gradient in line with the shaft center position, i.e., the radial film stiffness, is zero. No restoring force exists and

and the shaft is therefore inherently unstable It is essential, therefore, to determine the angle between the load and shaft displacement vectors in order to determine the stiffness. The film stiffness at zero load is especially important since it typically represents the lower limit.

Seven bearing configurations have been studied during this first quarterly reporting period with the objective of evaluating film stiffness and load carrying capacity. These include:

a. Cylindrical bearing with two axial grooves.

b. Preloaded cylindrical bearing (nut cracker)

c. Three lobe bearing.

d. Compound cylindrical.

e. Orthogonally displaced elliptical bearing.

f. Pivoted pad bearing.

g. Rayleigh step (journal) bearing.

Details of the analysis and results are discussed in a subsequent section, "Technical Discussion". Generally, however, the analysis uses existing computer solutions which properly applied or combined yield a solution for the particular bearing configurations under study. The compound cylindrical bearing, for example, is studied as the superimposed effects of three individual, adjacent cylindrical bearings. The shaft has a different eccentricity with respect to each bearing segment. For a

given position of the shaft in the compound bearing, each of the individual segment eccentricities can be calculated. Using the computer solution results of Reference 1, the individual load capacities of each bearing segment is determined. The results are combined vectorially to yield the dimensionless load capacity and angle to the line of centers. An IBM 650 computer program has been written to perform the detailed calculations and has been verified by hand calculations for two cases. Equations have been developed and a computer program written for the Rayleigh step (journal) bearing.

B. DESIGN IMPROVEMENTS

Basically the test rig design, as proposed, has not been changed. However, in the three month design period several complete layouts of the test rig have been prepared for test shaft diameters of 1; 1.25 and 1.5 inch. During these studies, several improvements of the test rig components were made. In Figure 4 the latest layout of the test rig designed for a test shaft diameter D = 1.25 ϕ inch is shown. The improvements made are as follows:

1. The overhung electrical motor of the drive spindle has been replaced by a drive spindle with a mid-span arrangement of the E-Motor between the bearings. The continuous power output was increased from 10 HP to 15 HP and the Class A motor insulation was changed to Class B for higher operating temperature capability.

2. The instrumentation section which connects the drive spindle housing with the test section has been completely redesigned for maximum

rigidity, good accessibility for alignment of the torque instrumentation gear, attachment of quill shaft to test shaft, and ability to set selected rotating unbalances.

3. Also the ridigity of the bearing housing has been increased. The capacitance gauges have been directly installed in the bearing housing, obtaining thereby, a vibration insensitive mounting which also minimizes read-out errors due to differential thermal expansion. All various bearing configurations can be installed in the same bearing housing, including the flexibly mounted bearings.

Parasitic torques will be generated if the lubricant on its path to the sump contacts the small flywheels on the overhung shaft. Lubricant deflectors have been provided to prevent this contact. A guard ring installed in the lubricant collector, which is inserted into the bearing housing, minimizes damage in case of high speed quill shaft rupture.

The bearing housing flanges have been extended above the support flanges. In this way it is possible to bolt the bearing housing directly to rigid supports and to attach additional masses if required.

4. For vertical position testing of shafts with large flywheels, a lubricant deflector has been installed in the bearing housing support below the upper partial bearing. This deflector has a function similar to that in Item 3 above.

5. The end cover has been provided with a lubricant sump. Also a shaft stop has been included which minimizes damage of test shafts in case of quill shaft rupture at high speeds.

6. For safety reasons, a snubber has been installed between the bearings. This device prohibits excessive deflection when the test shafts are driven through their natural frequencies.

7. Proper mounting and adjusting of the capacitance gauges can be obtained entirely from outside of the test rig. The design of the air passages surrounding the gauges as shown in Figure 4 provides maximum protection against moisture which tends to intrude in between the measuring areas. This moisture would disturb the capacitance gauge output signals.

IV. TECHNICAL DISCUSSION

A. BEARING INSTABILITIES

Problems in dynamic operation of bearings can arise from three different sources: (1) half frequency whirl, (2) synchronous whirl, (3) resonant whip. Since even the technical literature does not always distinguish between these phenonena, a review of their causes and effects is desirable.

1. Half-Frequency Whirl

This is an instability of the fluid film of the bearing. It is characterized by a whirl of the journal centers at a speed of approximately half the shaft rotational speed. It is shown in the literature (Reference 7, for example), that the dynamical equations of motion for a rotating shaft can be satisfied either by a stationary shaft center or by a shaft center-whirling at one-half shaft speed. Poritsky, (Reference 8) derives a criterion for evaluating the onset of instability, i.e., half frequency whirl. Bocker and Sternlicht (Reference 6) modified Poritsky's theory to apply to finite bearings. It was pointed out that the threshold of instability depends upon the radial component of the hydrodynamic fluid force, i.e. the film stiffness. Under certain conditions, such an instability may occur even at very low speeds. Good agreement was reached between theory and experiment for the case of translatory whirl in a vertical, stiff-shaft machine in which the bearings possessed a high degree of symmetry.

2. Synchronous Whirl

This is a forced vibration of the journal which is caused by a rotating load such as an unbalance. Its frequency is equal to the rotational speed of the shaft. Its magnitude depends upon the amount of unbalance, the shaft mass and deflection characteristics, lubricant film stiffness and damping. Its effect upon bearing force transmission has been studied and reported in Reference 9 and 10.

3 Resonant Whip

In some instances, a shaft instability occurs which has a frequency corresponding to the first system critical, even though the shaft is rotating at a substantially different speed. In Reference 8, Poritsky's analysis showed that such an instability would occur only at speeds exceeding twice the first system critical speed.

In both synchronous whirl and half-frequency whirl, the stiffness of the bearing configurations is an important parameter. In Reference (6), for example, the radial stiffness of two test bearings was calculated and measured experimentally. The results were than applied to predict the onset of half-frequency whirl in the translatory mode, i.e. in which the shaft axis translates so as to form a right cylinder. Theory and experiments agreed within 3.7% when using a graphically derived film spring constant.

It must be noted that this good agreement occurred with bearings which fulfilled a basic assumption in the analysis, i.e. of a high degree

of symmetry. In the present study, however, this degree of symmetry does not always exist. In a two axial groove bearing, for example, the stiffness will depend upon the position of the load vector. As the load moves into the axial feeding slots, the stiffness approaches zero. The effect of this variation is not presently known. One purpose of the experimental investigation in Phase I of the subject program is to correlate such analytical information with the behavior of the bearings under test.

B. ANALYSIS OF CONFIGURATIONS

As stated earlier, the analysis of the bearing configurations uses existing computer solutions which must be properly combined and applied to given solutions for many of the non-symmetrical complex geometries analyzed. The basic existing computer solutions do not always cover a complete range of bearing length/diameter ratios. Calculations for the configurations proposed in this program have been carried out so far with the data presently availalble on length/diameter ratios. The cyclical variation of film stiffness can be expected to differ in magnitude, but not essentially in form for similar bearings with different length/diameter ratios. For the preliminary selection of bearings in Phase I, a complete analysis of film stiffness with variation of all possible parameters does not presently appear justified. Film stiffness itself is only one of the possible parameters affecting stability for the non-symmetrical bearings studied.

Zero load radial stiffness and load carrying capacity at a minimum film thickness of .0005 inches, (which was considered to be a minimum practical working value from the standpoint of tolerances, distortions, dirt, etc.) have been calculated for several of the bearing types under consideration. The dimensionless parameters used to express these two quantities are:

Load capacity parameter $\left(\frac{W}{D^2 \mu N}\right)$

Stiffness parameter $\left(\frac{W}{D \mu N}\right)$

where a typical set of units would be:

D = inch
K = lb/inch
N = rev/sec
W = lb
μ = lb. sec/in^2

1. Two Groove Cylindrical Bearing

This was calculated by compounding two partial arc bearings each having an arc of 150°, the basic data being obtained from Reference 1. The maximum stiffness and the load capacity are shown, these falling to zero as the loading vector departs from the central position.

Load capacity at .0005 inch minimum film thickness: (Maximum values)

$(W/D^2 \mu N) \times 10^{-6}$

	L/D	.5	1.0	1.5
C/D	.0016	.217	1.26	3.0
	.0028	.263	1.25	2.33
	.0040	.260	1.12	1.87

Radial stiffness ($\Sigma \rightarrow 0$) (Maximum values)

$(K/D\ \mu N) \times 10^{-10}$

	L/D	.5	1.0	1.5
C/D	.0016	.0222	.126	.355
	.0028	.00414	.0235	.0663
	.0040	.00142	.00806	.0227

2. Preloaded Cylindrical Bearing (Nut Cracker)

The low values of radial stiffness in a plain or grooved cylindrical bearing are due to the relatively high value of the Sommerfeld number at low eccentricity as well as the high attitude angle between the applied load and the resulting shaft displacement (Approaches 90 degrees). Both of these effects are improved if the eccentricity is increased by preloading. The increased stiffness is obtained at the expense of load carrying capacity by an amount equal to the preload. The preloading also fills in the "holes" of stiffness as a function of load direction to a large extent; maximum and minimum values of stiffness are shown in the table. The amount of preloading is, of course, a controllable variable,

and the amount of preloading used in this example is sufficient to produce an initial eccentricity of 0.5 in the two groove cylindrical bearing of 1. No value of load capacity is listed at the lowest clearance ratio because the minimum film thickness of .0005 inch is exceeded by the preloading alone.

Load capacity at .0005 inch minimum film thickness:

$$(W/D^2\mu N) \times 10^{-6}$$

	L/D	.5	1.0	1.5
C/D	.0016		---	
	.0028		.641	
	.0040		.818	

Radial Stiffness ($\Sigma \rightarrow 0$)

$$[(K/D\ \mu N)\ \text{min}/\ (K/D\mu N)\ \text{max}] \times 10^{-10}$$

	L/D	.5	1.0	1.5
C/D	.0016		.127/.538	
	.0028		.0237/.100	
	.0040		.00812/.0344	

Although an L/D of unity was the only value computed, other values would compare similarly to the two groove cylindrical bearing. In general, the stiffness increase and the load capacity at minimum film thickness decreases as more preloading is applied.

3. Three Lobe Bearing

The "nut cracker" bearing described above achieved preloading by the actual application of a force from an auxiliary opposed bearing. Preloading may also be achieved by offsetting opposing sides of a single bearing. The first method can be thought of as force preloading, and the second method as displacement preloading. The three lobe bearing is of the latter type and consists essentially of three eccentric lobes, the center of each lobe displaced an equal distance, called the ellipticity, from the center of the bearing, thereby producing in most cases, three active hydrodynamic wedges. The bearing shown here has three symmetrical lobes of 100 degrees of arc with an ellipticity equal to one half of the lobe clearance. The stiffness is almost independent of the direction of the loading vector in contrast to the above two types. Load capacity is not listed for the smallest eccentricity as the minimum allowable film thickness is already exceeded at zero load. The source from which this data was computed is Reference 2.

Load capacity at .0005 inch minimum film thickness:

$(W/D^2\ \mu N) \times 10^{-6}$

L/D		.5	1.0	1.5
C/D	.0016	---		
	.0028	.0903		
	.0040	.115		

Radial Stiffness ($\Sigma \rightarrow 0$)

$(K/D\ \mu N) \times 10^{-10}$

	L/D	.5	1.0	1.5
C/D	.0016	.113		
	.0028	.0221		
	.0040	.00725		

4. Orthongonally Displaced Elliptical Bearing

This configuration is a two lobe version of the above bearing, each lobe having not only an elliptical displacement, but also a displacement normal to the ellipticity. A bearing having an L/D ratio of 1/2 with an ellipticity and displacement equal to 0.5 times the lobe clearance is analyzed in Reference 3. Maximum zero eccentricity radial stiffness is approximately 45 times the value of the two groove bearing, but similar to the two groove bearing, the stiffness is positive for only two sectors of load direction, each about 75° wide. Load capacity is less than for a two groove bearing of the same lobe clearance ratio due to the built in eccentricity. The exact effects of the "holes" in the stiffness versus load direction on the shaft stability is unknown, so due to the constructional simplicity of this configuration this design will merit testing.

5. Pivoted Pad Bearing

A four pad pivoted pad bearing was analyzed using the methods and data of Reference 4 which, based on experimental evidence, assumes an attitude angle of zero.

Load capacity at .0005 inches minimum film thickness.

$$[(W/D^2\ \mu N)\ \max/(W/D^2\ \mu N)\ \min]\ \times\ 10^{-6}$$

	L/D	.5	1.0	1.5
C/D	.0016	.0449/.0650		
	.0028	.124/.1765		
	.0040	.137/.1895		

Radial Stiffness $(\Sigma \rightarrow 0)$

$$(K/D\ \mu N)\ \times\ 10^{10}$$

	L/D	.5	1.0	1.5
C/D	.0016	0.058		
	.0028	0.0108		
	.0040	0.0037		

Although the load capacity is a function of load direction, the zero eccentricity stiffness is quite independent of direction.

6. Compound Cylindrical Bearing

This bearing is a variation of the three lobe bearing. Although simpler to manufacture than the three lobe design, it is probably heavier and has a greater overall length for a given load capacity. The stiffnesses are as follows:

$(K/D\ \mu N) \times 10^{-10}$

(L/D) Lobe	.5	1.0	1.5
C/D .0016	.352		
.0028	.0656		
.0040	.0225		

The L/D ratio listed above is for a single element of the bearing, the overall length being three times this value. Load capacity is presently being calculated.

7. Rayleigh Step Bearing

This design has been analyzed and programmed for an IBM 650 computer, but as yet only preliminary results are available. A very low attitude angle is indicated by these results, and computations are being continued.

C. MECHANICAL DESIGN OF TEST RIG COMPONENTS

1. Selection of Bearing Clearances

It is desirable in the tests to duplicate as many of the variables as possible that would influence the performance of hydrodynamic liquid metal lubricated bearings in space power plants. Bearing performance strongly depends on clearances, as well as such variables as bearing configurations, diameter and length, rotor mass and rotor inertia moments, lubricant supply pressure, etc.

Distilled water which will be mainly used as bearing lubricant during the experimental evaluation has slightly different viscous properties than liquid potassium or sodium. Considering the Sommerfeld and Taylor numbers,

$$\text{Sommerfeld No.} = \frac{\mu N}{P}\left(\frac{D}{C}\right)^2 ; \qquad \text{Taylor No.} = \frac{2\pi}{\nu}\left(C^3 R\right)^{1/2}$$

which characterize bearing performance and turbulence, it is possible to nearly match the two characteristic numbers by a corresponding large proportional difference between the bearing clearances used in the test and those used in the applications. In Figure 5, the Sommerfeld and Taylor numbers are compared. The applicable fluids are liquid potassium, as well as liquid sodium in the temperature range 600° to 1200°F, while the test fluid is distilled water in the temperature range 100° to 170°F. The comparisons are made for speeds of 18,000, 24,000, and 36,000 rpm. Bearing clearance ratios for sodium or potassium lubricated hydrodynamic bearings usually are in the range from $\frac{C}{R}$ = 0.001 to 0.0025 inch per

inch. Using the Sommerfeld and Taylor number as criteria, the clearance ratios for water lubricated bearings range then from 0.0016 to 0.004 inch per inch. For convenience of presentation, a load of 25 psi was used for the water lubricated bearings having a clearance ratio of 0.0016 inch per inch. However, since the load will be equal in both applications and tests, its magnitude will not effect the comparisons.

As Figure 5 shows, the range of both characteristic numbers are quite closely matched between application and test. In almost all cases, the characteristic numbers of water lubricated bearings are between those of potassium and sodium lubricated bearings. The deviations between the different characteristic numbers decrease with large bearing clearance ratios and increase at higher speeds. The three selected test bearing clearance ratios are:

For Water $C/R = 0.0016 \qquad 0.0028 \qquad 0.004.$

These ratios closely resemble the following clearance ratios for liquid potassium or sodium lubricated bearings:

$C/R = 0.001 \qquad 0.00175 \qquad 0.0025.$

2. Power Requirements of Test Rig

The power limitation of the test rig drive motor requires the investigation of maximum torque and power losses which occur in the test rig. At this stage, an exhaustive and accurate calculation of bearing

losses is not yet possible, because not all test bearing configurations have yet been selected. However, a fairly accurate estimation of the highest and also the lowest (required for the selection of the quill shafts) power requirements of the test rig can be made. It can then be expected that most bearing tests will fall between these two extreme limits.

Approximately the highest power loss will occur when:

H_{max} = 2 x test bearing loss (L/D = 1.5; C/R = 0.0016, $\frac{\text{Bearing Load}}{\text{Bearing}}$ = 200 lb).

+ 2 x Loader Bearing Loss (L/D = 1.5; C/R = 0.0016; $\frac{\text{Bearing Load}}{\text{Bearing}}$ = 200 lb).

+ Spindle Windage Losses (Heavy rotor, distance between bearing centers c = 12.5 inch)

+ [2 x motor bearing loss + motor rotor windage loss].

Minimum power losses can be expected when:

H_{min} = 2 x Test Bearing Loss (L/D = 0.75; C/R = 0.004).

+ Spindle windage losses, distance between test bearing center = 7.5 inches).

+ [2 x Motor Bearing Loss + Motor Rotor Windage Loss].

The losses due to the motor bearings and rotor windage have been enclosed in brackets since these losses do not effect the torque which has to be transmitted through the quill shaft.

The Petrow equation has been used to calculate the hydrodynamic bearing power losses. However, since the bearings are lubricated with distilled water and operate at speeds up to 35,000 rpm, it can be expected that the load supporting lubricant film becomes turbulent above a certain speed. According to Taylor (Reference 12) speed and bearing clearance effects the transition from laminar to turbulent lubricant film operation. Figure 6 indicates the transition speed for the unloaded test bearings as a function of bearing clearance ratio and water viscosity. As an indication how close water lubricated bearings can match the characteristics of liquid potassium lubricated bearings, the transition speed of these bearings are also plotted in the same Figure.

As experiments (Reference 13 and 14) have indicated, hydrodynamic bearing losses increase considerably when the lubricant film becomes turbulent. Though accurate power loss calculations for bearings which operate in the turbulent region cannot yet be obtained due to insufficient experimental and analytical data, the presently best available information (Reference 15 and 16) has been employed to determine the power losses of the cylindrical and partial bearings of the test rig. As indicated before, the bearing losses have been determined on the basis of laminar lubricant flow and have been corrected by a power factor, Kp, in order to obtain the losses occurring due to operation in the turbulent region.

Basically the power coefficient is a function of the bearing Reynolds number which is defined as:

$$Re = \frac{2\pi R N . C}{\nu}$$

In any loaded bearing, however, the viscosity and the clearance vary along the lubricant layer and the transition from laminar to turbulent film flow usually does not occur immediately at the critical Reynolds number $Re_c = \sqrt{\frac{41.1}{C/R}}$.

As a first approximation for water lubricated bearings, it has been assumed that the viscosity remains constant so that the critical Reynolds number of a loaded bearing occurs at:

$$Re_m - \frac{h_o}{c} \quad Re_C$$

where:

$$\frac{h_o}{C} \cong 2 \frac{1 - n^2}{2 + N^2} .$$

In this case, Re_m decreases with n.

For the laminar region, the bearing losses are:

$$H_L = j \frac{2\pi^3 \mu N^2 D^3 L}{C_D} .$$

For the turbulent region:

$$H_T = K_p . H_L = K_p . j \frac{2\pi^3 \mu N^2 D^3 . L}{C_D} .$$

Figure 7 shows the power factor K_p as a function of the bearing Reynolds number.

The correlations of Reference 11 have been used to determine bearing spindle and motor rotor windage losses.

For the test rig having a 1.25" bearing diameter, Figure 8 indicates the maxima and minima power requirements which have to be transmitted by the quill shaft. (Motor rotor windage and motor bearing losses have not been included.)

Detailed power loss calculations for a range of bearing diameters (D = 1" to 2") have been obtained for N = 35,000 and 30,000 rpm. This work became necessary during the investigation of the dynamic characteristics of various test shaft configurations, (see Section 4). In Figure 9, cylindrical and partial bearing losses are plotted versus bearing diameters. Both bearings support a 200 lb unidirectional load. As the curves indicate, the power losses increase with larger diameters at a considerably higher rate during turbulent operation as compared to laminar operation. In the laminar region, the losses should rise as a function of $(D/D)^3$ for constant (C/R) ratio and viscosity.

The assumption that the viscosity of the lubricant fluid remains constant tends to yield rather conservative bearing power losses. It should, however, be realized that with decreasing viscosity the intensity of turbulence in the lubricant film tends to increase. This can offset the effect of lower viscosity.

Figures 10 and 11 show a detailed breakdown of losses as they occur in the different components of the test rig. Bearing spindle windage is calculated for the heavy test rotor and the bearing ℄ to ℄ distance of 12.5 inch. The losses occurring the the grease packed ball bearings of the rotor spindle are based on conservative estimates

3. Quill Shaft Design

Figure 8 indicates the range of power (from 0.1 to 7.5 HP) which is required to drive the various 1.25 in. test shaft configurations at speeds ranging from 3500 to 35,000 rpm. Quill shafts are employed to mechanically transmit the resulting torque from the motor spindle to the test bearing shaft. Several limitations are imposed upon the quill shaft.

a. Quill shaft should not impair free movement of test shaft. This favors the selection of a very flexible small diameter shaft.

b. Angular deflection of quill shaft has to be larger than 3°, but should not exceed 20°. A deviation from these limits impairs accurate torque measurement.

c. The combined stresses occurring in the quill shaft should be kept as low as possible in order to minimize the danger of quill shaft rupture.

Figure 12 indicates the angular deflection of various sized quill shafts for the torque range corresponding to the power required to drive the various test shaft configurations, (see Figure 13). As the results indicate, at least four different sized quill shafts are required, if bearing

investigations are to be extended into the low speed region; two different sized quill shafts should be sufficient to test in the high speed region.

The largest quill shaft which the test rig can accommodate has a 0.1875 inch diameter. Figure 12 also indicates the 40,000 psi combined stress level which will occur first in the larger diameter quill shafts. This stress level has tentatively been chosen as an upper allowable stress limit. The stress calculations included stress due to tension, angular twist and bending due to misalignment between spindle and test shafts. The maximum alignment amounts to a radial run-out of 0.0025 inch, which in turn corresponds to an eccentricity n = 1 of a bearing having a clearance ratio C/R = 0.004 inch/inch. Figure 14 shows the combined quill shaft stress as a function of quill shaft diameter. In Figures 15 and 16 the combined stress of a misaligned and an aligned quill shaft have been compared as a function of angular deflection. The stress calculations support the expectation that, for the same angular deflection, the stresses increase rapidly with increasing shaft diameter.

4. Natural Frequency of the Shaft-Bearing System

In the proposed analytical and test programs, it is desirable to treat the shaft as a rigid body. This means that the stiffness of the shaft should be much greater than that of the selected bearing configurations. Due to the problems associated with measurements and analysis of the shaft-bearing dynamics induced by the lubricant, the shaft natural frequencies

should occur, if possible, above the speed range of interest. Since critical shaft speeds depend strongly on length and diameter of the shaft and upon the distribution and magnitude of the rotating masses which are attached to the shaft, a detailed study has been carried out to investigate their effects. Table 1 shows the results of calculations which have been carried out for various test shaft configurations using an existing IBM 7090 program.

As the table indicates, the bearing film stiffness which has to be assumed for the computer program has a considerable effect on the natural shaft frequencies. Compared to the simply supported flexible shafts, the critical speeds of shaft configurations which included the effect of bearing film stiffness were progressively lower with decreasing film stiffness. Also, with increasing shaft diameter or with increased mass, the decreasing effect of film stiffness becomes more pronounced. Figure 17 gives the explanation why this is so. Here the critical speed for an infinite rigid shaft supported on springs is compared to simply supported flexible and spring supported flexible shafts. While the critical speed of the simply supported flexible shafts increases with larger diameters, the natural frequency of the flexibly supported rigid shafts decreases. Actually, a combination of both supports occurs in reality for high speed shafts supported by hydrodynamic bearings. As Figure 17 indicates, due to the conflicting trend of the two previously discussed types of supports, the critical speed of a spring supported flexible shaft increases at a much lower rate compared to that of a simple supported flexible shaft with increasing diameter. An exact analytical determination of the actual

TABLE I

CALCULATED CRITICAL SPEEDS [RPM]

SHAFT DIAMETER [inch]	SHAFT SPAN [inch]	FILM STIFFNESS [lb/inch]	CRITICAL SPEED: HINGED - HINGED	CRITICAL SPEED: RIGID SHAFT ON SPRINGS	CONFIGURATION
1.0	12	1×10^5	-----	1. Critical = 16,314 2. Critical = 25,482 3. Critical = 32,469	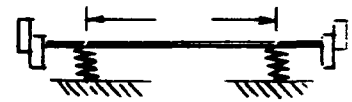
1.0	12	-----	1. Critical = 17,565 2. Critical = 34,971	-----	
1.0	12	-----	1. Critical = 14,721 2. Critical = 30,240	-----	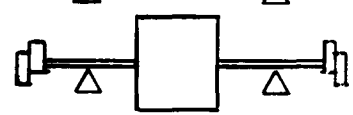
1.25	12.5	-----	1. Critical = 27,147	-----	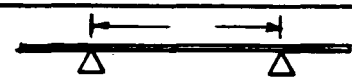
1.25	12.5	-----	1. Critical = 24,845	-----	
1.25	12.5	-----	1. Critical = 33,889	-----	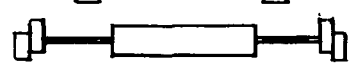
1.25	12.5	$.5 \times 10^5$	-----	1. Critical = 15,697 2. Critical = 20,770 3. Critical = 26,719	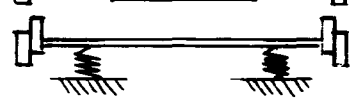
1.25	12.5	1×10^5	-----	1. Critical = 19,665 2. Critical = 27,574 3. Critical = 29,541	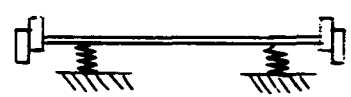
1.25	12.5	5×10^5	-----	1. Critical = 23,522 2. Critical = 39,492	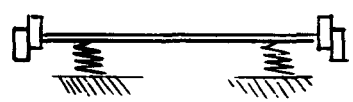

TABLE I (contd)

CALCULATED CRITICAL SPEEDS [RPM]

SHAFT DIAMETER [inch]	SHAFT SPAN [inch]	FILM STIFFNESS [lb/inch]	CRITICAL SPEED HINGED - HINGED	CRITICAL SPEED RIGID SHAFT ON SPRINGS	CONFIGURATION
1.5	12.5	-----	1. Critical = 34,713	-----	
1.5	12.5	0.5×10^5	-----	1. Critical = 16,664 2. Critical = 18,853 3. Critical = 35,622	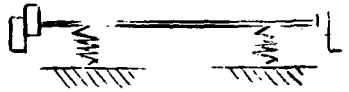
1.5	12.5	1.0×10^5	-----	1. Critical = 23,226 2. Critical = 26,004 3. Critical = 36,120	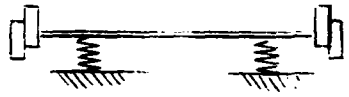
1.5	12.5	5×10^5	-----	1. Critical = 34,370	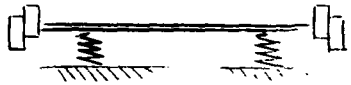
1.25	7.5	-----	1. Critical = 33,159	-----	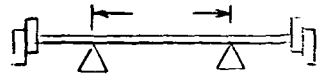
1.25	7.5	1.0×10^5	-----	1. Critical = 19,170 2. Critical = 30,032	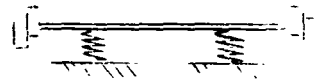
1.25	7.5	-----	1. Critical = 29,919	-----	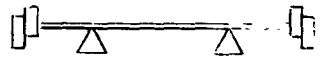
1.5	7.5	-----	1. Critical = 55,964	-----	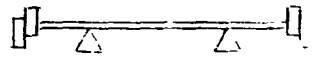
1.5	7.5	1×10^5	-----	1. Critical = 21,436 2. Critical = 28,939	

bearing film stiffness present at the outset of the natural shaft frequency is impossible due to many uncontrollable variables. Realistic film stiffnesses as they might occur in water or liquid metal-lubricated, lightly-loaded, hydrodynamic bearings should range between 1×10^5 and 5×10^5 lb/inch.

On this basis, as shown in Table 1 and Figure 17, the test shaft diameter has to exceed at least 1.5 inch in order that the first rotor critical speed occurs above 35,000 rpm. Due to the power limitation of the electrical motor drive (15 HP at 36,000 rpm), the effects of an increase in shaft diameter require careful examination. As already discussed in Chapter 2 , with increasing diameter, power losses in the bearings rapidly approach the drive motor power limit. Furthermore, a certain amount of driving power has to be reserved for acceleration; Figure 19 indicates the amount of driving power required to accelerate the rotating test rig components from 30,000 to 35,000 rpm.

The first critical shaft speed can be raised above 35,000 rpm, by increasing the diameter of the shaft section between the bearings. However, this approach has not been used because it requires disassembly of the bearing test rig when changing the test shaft configuration. This impairs accurate realignment of the bearings. As Figure 18 shows a slight increase of the natural shaft frequency can be obtained with hollow shafts; however, the small improvement is easily offset by manufacture and balancing problems. Every care has been taken to minimize the necessary shaft overhang and the weight of the eccenters which are used to generate rotational loads.

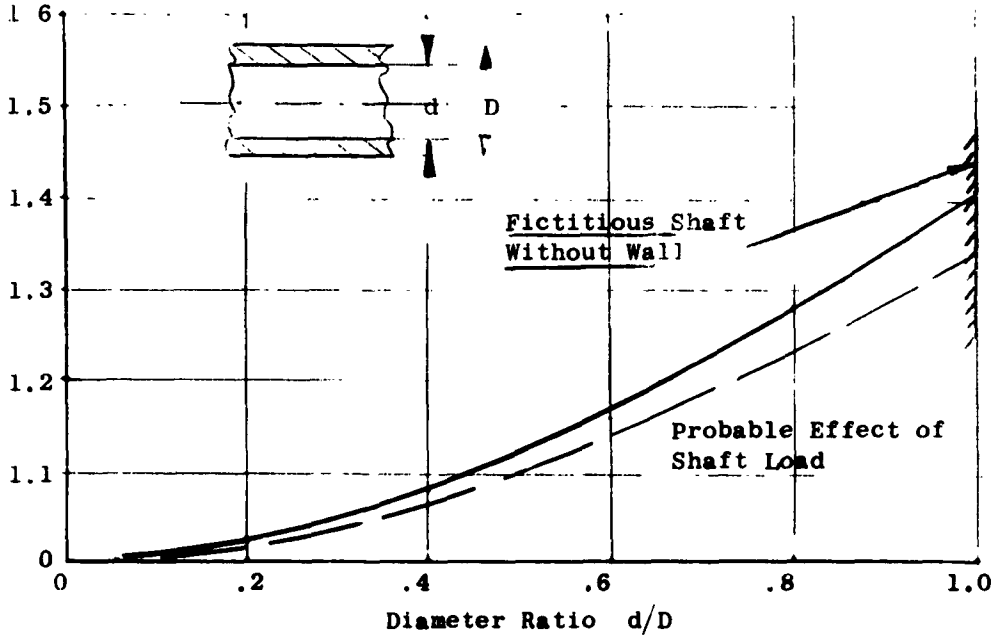

Figure 18. Ratio $\frac{\text{Natural Frequency of Hollow Shaft}}{\text{Natural Frequency of Solid Shaft}}$ vs. Diameter Ratio.

The results of all the investigations done so far have been reported to the NASA project engineer. The NASA administration selected a 1.25 inch diameter shaft.

D. EXPERIMENTAL INVESTIGATION OF CAPACITANCE GAUGES

Capacitance proximity gauges are proposed as the basic shaft displacement sensing element. GEL experience with such gauges has been satisfactory when they have been used with instrumentation specifically modified to minimize drift. A potential problem with capacitance gauges exists, however, if water or water exists in the clearance space between the gauge head and the surface whose displacement is being measured. To eliminate this problem, it was postulated that the gauge head could be surrounded by a flow of air or dry gas blowing away any detrimental water vapor. An experimental capacitance gauge using this principle has been tested. It was found to retain its calibration and ability to keep the measuring area on a rotating spindle free from water.

1. Calibration With and Without Air Flow

In the experiment, such a capacitance gauge was calibrated for a full scale deflection with 0.005 inch displacement. Instrument reading versus change in displacement was measured both with zero air flow and with air at 15 psi. Calibration was virtually unaffected by air flow as shown in the tabulation below:

CAPACITANCE BRIDGE BALANCED AT 10 MILS CALIBRATION ON SENSITIVITY 3

Micrometer Reference	Mils Displacement	Volts (No Air)	Volts 15 psi, 1/2 Hr.	Volts 15 psi, 1 Hr.
3	0	5.88	5.86	5.86
4	1	4.16	4.12	4.12
5	2	2.96	2.92	2.92
6	3	2.09	2.06	2.07
7	4	1.41	1.37	1.39
8	5	.89	.87	..87

2. Air Flow Protection Against Moisture

Tests were also made to check the ability of the air flow to keep the measuring areas free from moisture. In these tests, the capacitance gauge was mounted with the sensing element horizontal and facing a spindle with negligible run-out. A glass funnel with a stop cock was mounted directly above the measuring area. Tests were conducted at various air pressures with water dropping on the rotating spindle (8000 rpm) just ahead of the capacitance gauges. Fluctuations in the gauge output were observed on an oscilloscope. It was found that an air pressure of 15 psi and a flow of 1.7 cfm was sufficient to keep the measuring area free from moisture and the gauge output signal clear.

V. NOMENCLATURE

C	=	Clearance [inch]
D	=	Diameter [inch]
H	=	Power Loss [HP]
K_p	=	Power Coefficient
L	=	Bearing Length [inch]
N	=	Speed [RPM]
R	=	Bearing Radius [inch]
Re	=	Reynolds Number defined by the inlet viscosity
j	=	Bearing Loss Factor
μ	=	Inlet Viscosity
ν	=	Kinematic Inlet Viscosity

Subscripts:

D	=	Diametral
L	=	Laminar
R	=	Radial
T	=	Turbulent

VI. REFERENCES

1. O. Pinkus, B. Sternlicht, "Theory of Hydrodynamic Lubrication," McGraw-Hill Company, 1961.

2. O. Pinkus, "Analysis of Arbitrarily Loaded 3-Lobed Bearings," G.E. Report R59MSD322.

3. D.F. Wilcock, "Orthogonally Displaced Bearings-I," ASME preprint 60LC-7. Also direct communication with Dr. Wilcock.

4. H. Ernst, "Tilted Pad Journal Bearing Design for a Potassium Vapor Turbine," G.E. Report R61FPD425.

5. B. Sternlicht, H. Poritsky, E. Arwas, "Dynamic Stability Aspects of Cylindrical Journal Bearings Using Compressible and Incompressible Fluids," Contract No. Nonr - 2844 (00). Task No. NR 097-348.

6. G.F. Bocker and B. Sternlicht, "Investigation of Translatory Fluid Whirl in Vertical Machines," ASME Paper No. 54-Lab-3.

7. Shaw & Macks, "Analysis and Lubrication of Bearings," McGraw-Hill Co., New York City, New York (1949).

8. H. Poritsky, "Contribution to the Theory of Oil Whip," Teans. ASME Vol. 75, 1953 - pp. 1153 - 1161.

9. J. Lund, B. Sternlicht, "Bearing Attenuation," Report No. 61GL100, April 28, 1961.

10. J.D. McHugh, J. Lund, "Bearing Attenuation - Experimental Evaluation," August 28, 1961, Contract No. Nobs. 78930 - Burear of Ships.

11. T. Theodorsen and A. Regier, "Experiments on Drag of Revolving Disks, Cylinders and Streamline Rods at High Speeds," NACA Report 793.

12. G.I. Taylor, "Stability of a Viscous Liquid Contained Between Two Rotating Cylinders," Philosophical Transactions, Series A., Volume 223, 1923.

13. M.I. Smith and D.D. Fuller, " Journal-Bearing Operation at Super-Laminar Speeds," Transactions ASME, April, 1956.

14. D.F. Wilcock, "Turbulence in High-Speed Journal Bearings," Transactions ASME, August, 1950.

15. V.N. Constantinescu, "On Turbulent Lubrication," Proceedings, I. Mech. Eng., Vol. 173, 1959.

16. V.N. Constantinescu, "Analysis of Bearings Operating in Turbulent Regime," ASME Paper No. 61- Lub. -5.

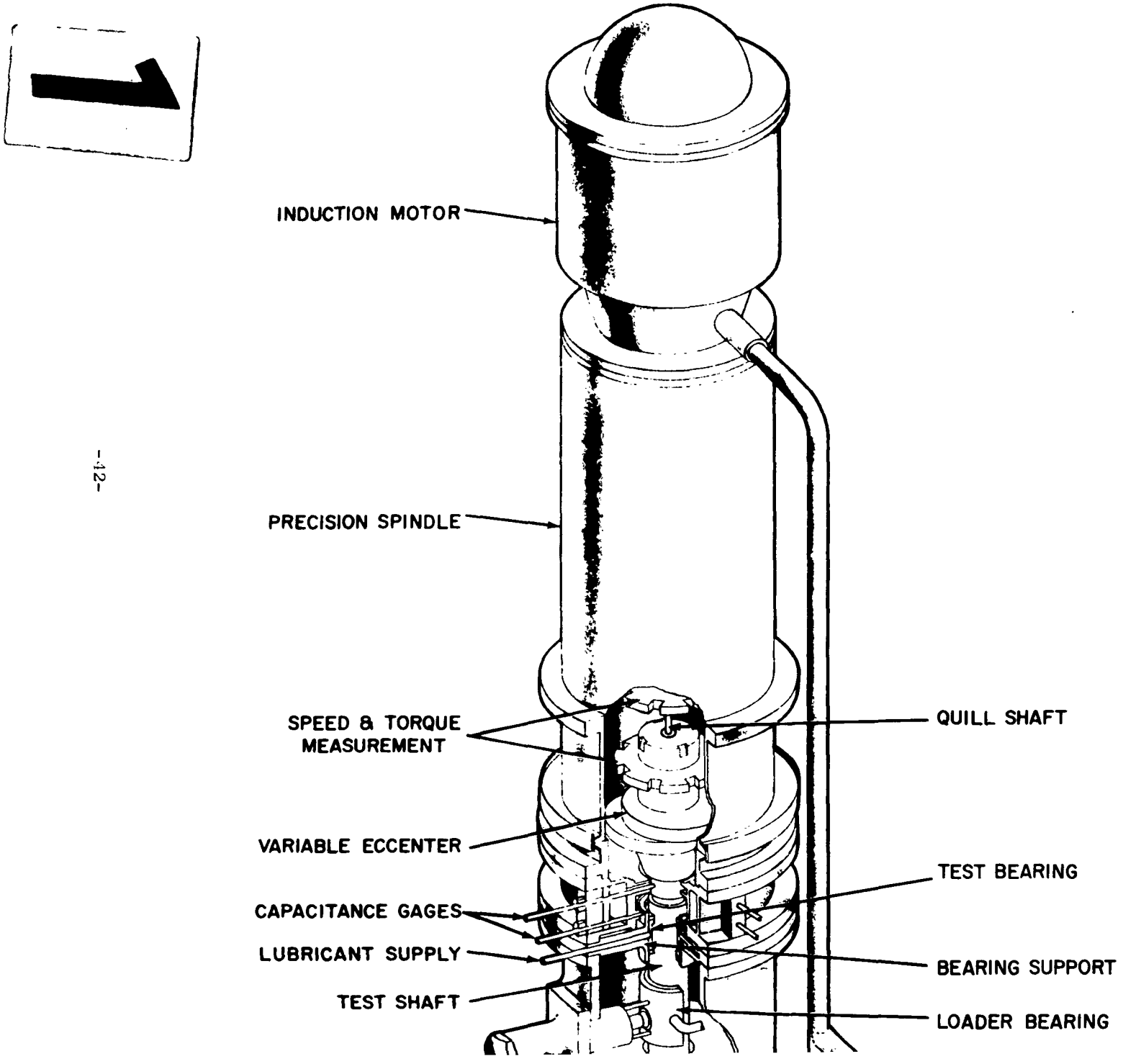
INDUCTION MOTOR
PRECISION SPINDLE
SPEED & TORQUE MEASUREMENT
QUILL SHAFT
VARIABLE ECCENTER
TEST BEARING
CAPACITANCE GAGES
LUBRICANT SUPPLY
BEARING SUPPORT
TEST SHAFT
LOADER BEARING

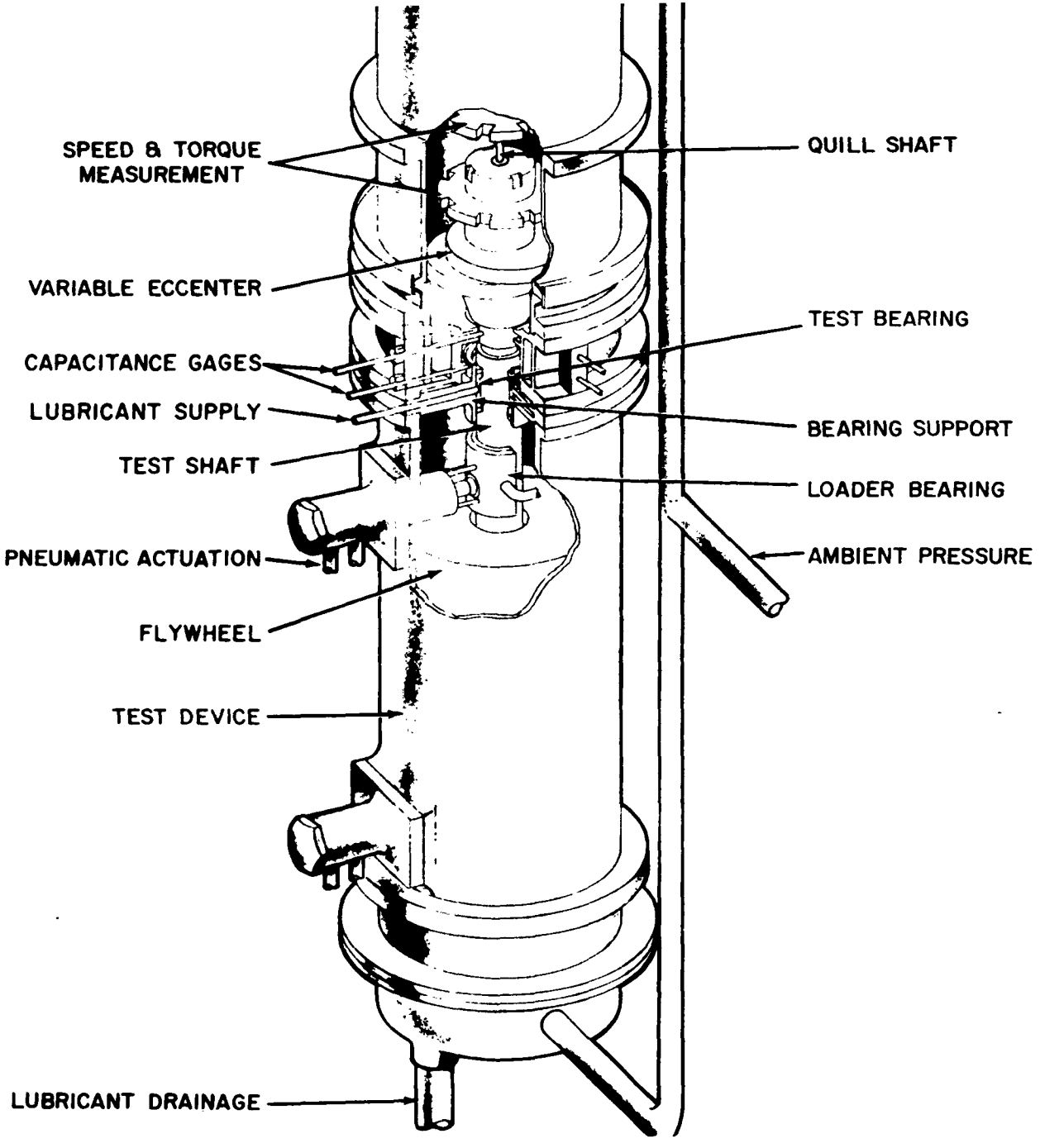

Figure 1 Isometric View of Bearing Stability Test Rig

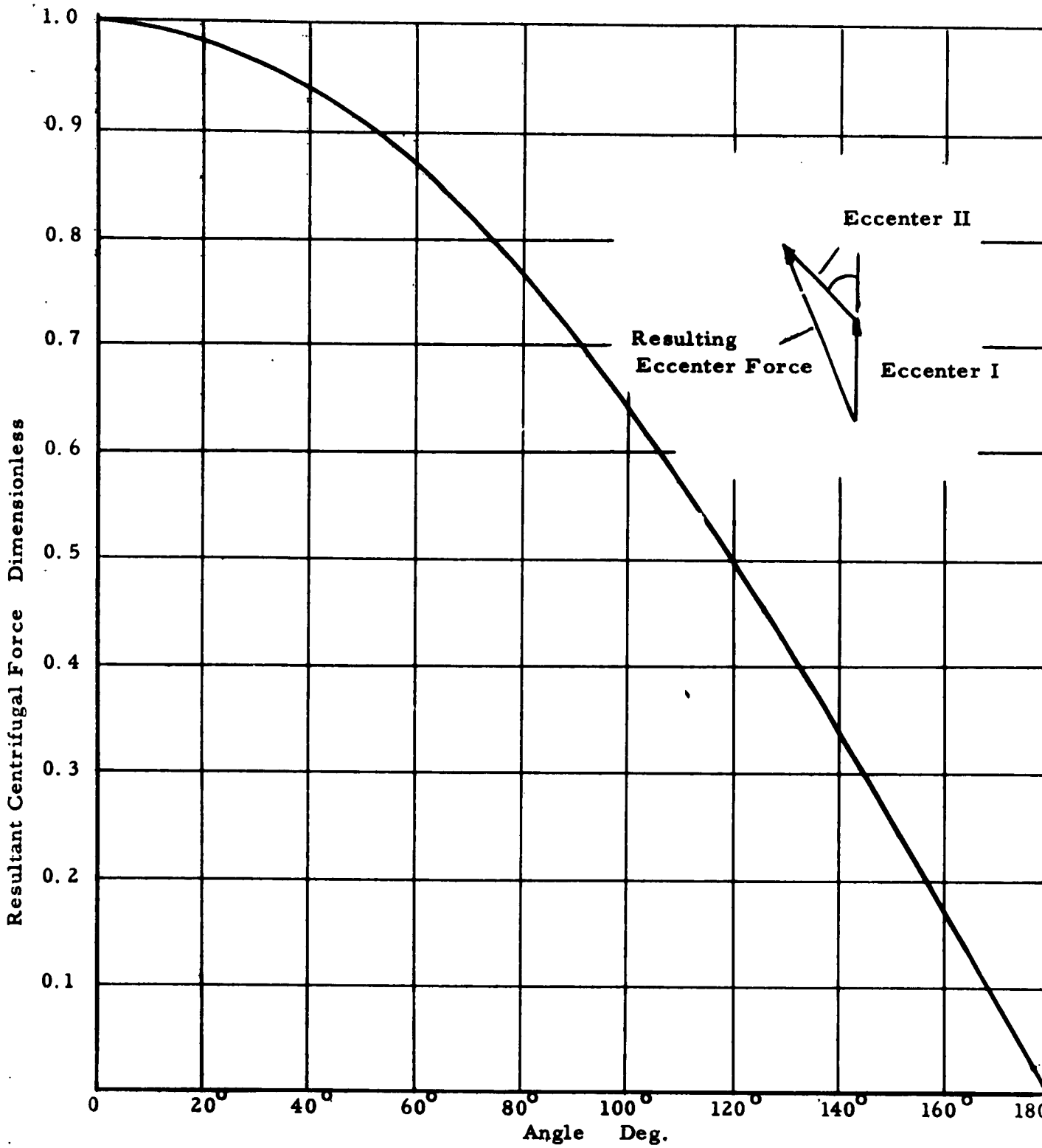

Figure 2. Resultant Centrifugal Eccenter Force vs. Angle.

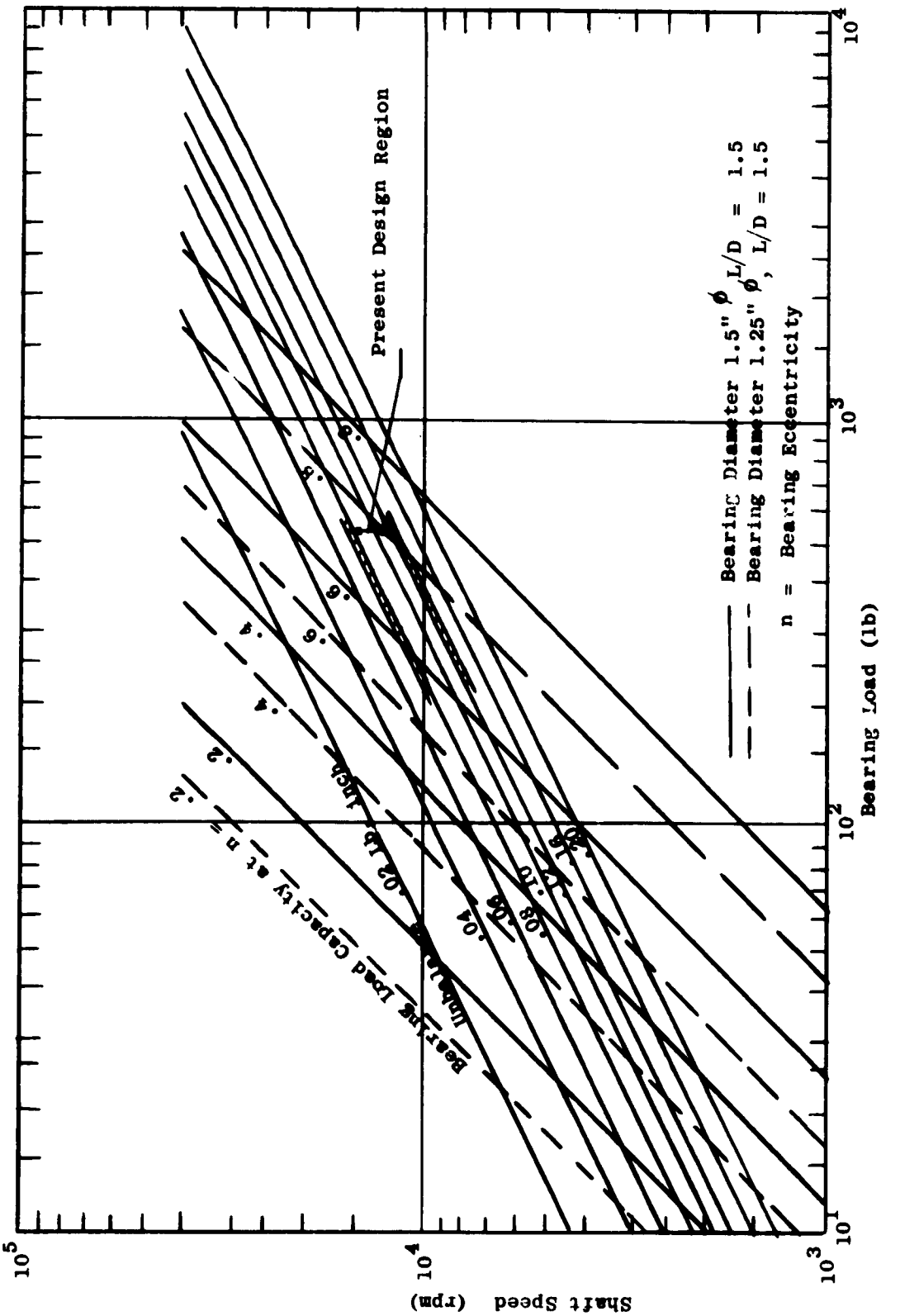

Figure 3. Bearing Strength and Bearing Load Due to Eccentricity vs. Shaft S

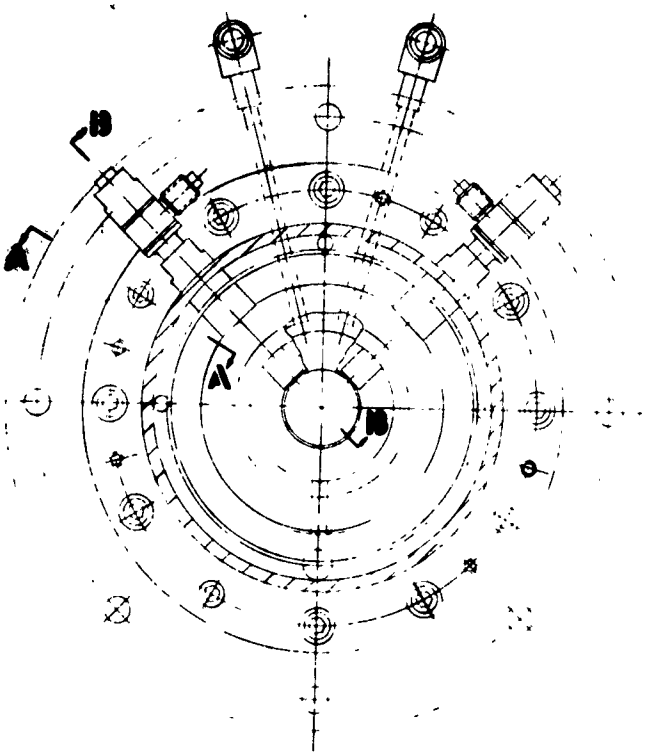

SECT C-C

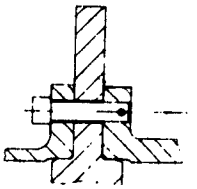

SECT A-A

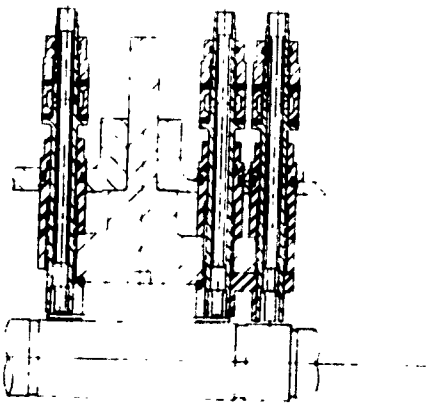

SECT B-B

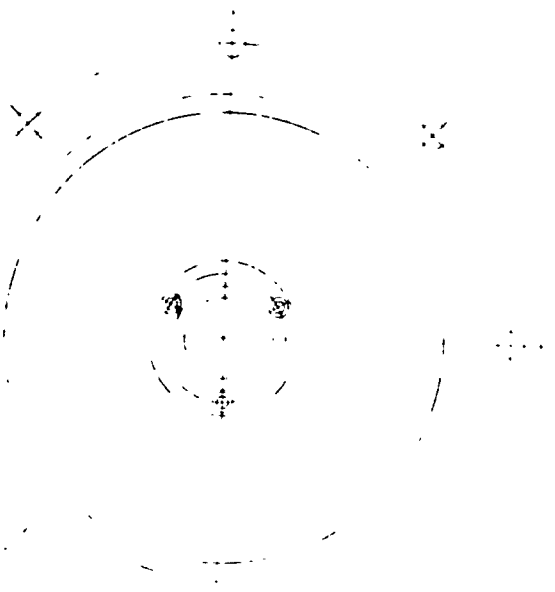

C

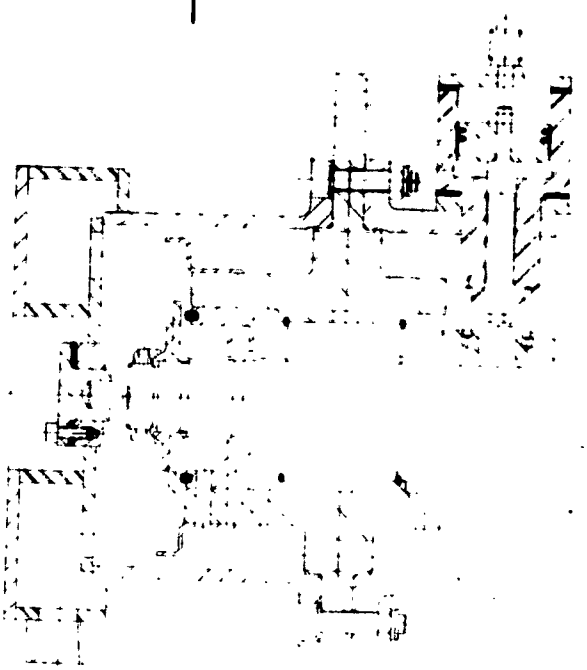

C

1

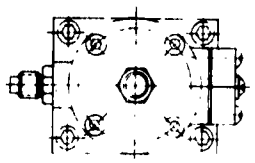

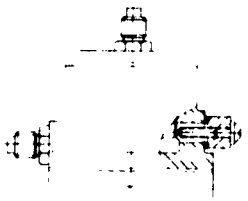

PART SECT D-D

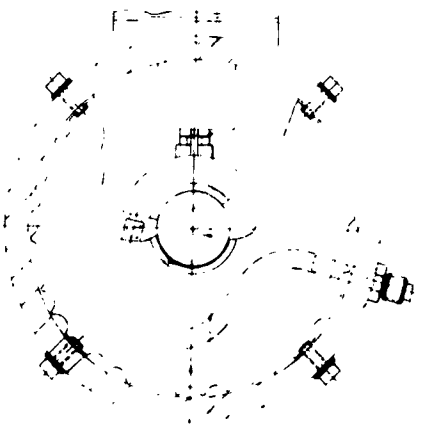

SECT E-E

2

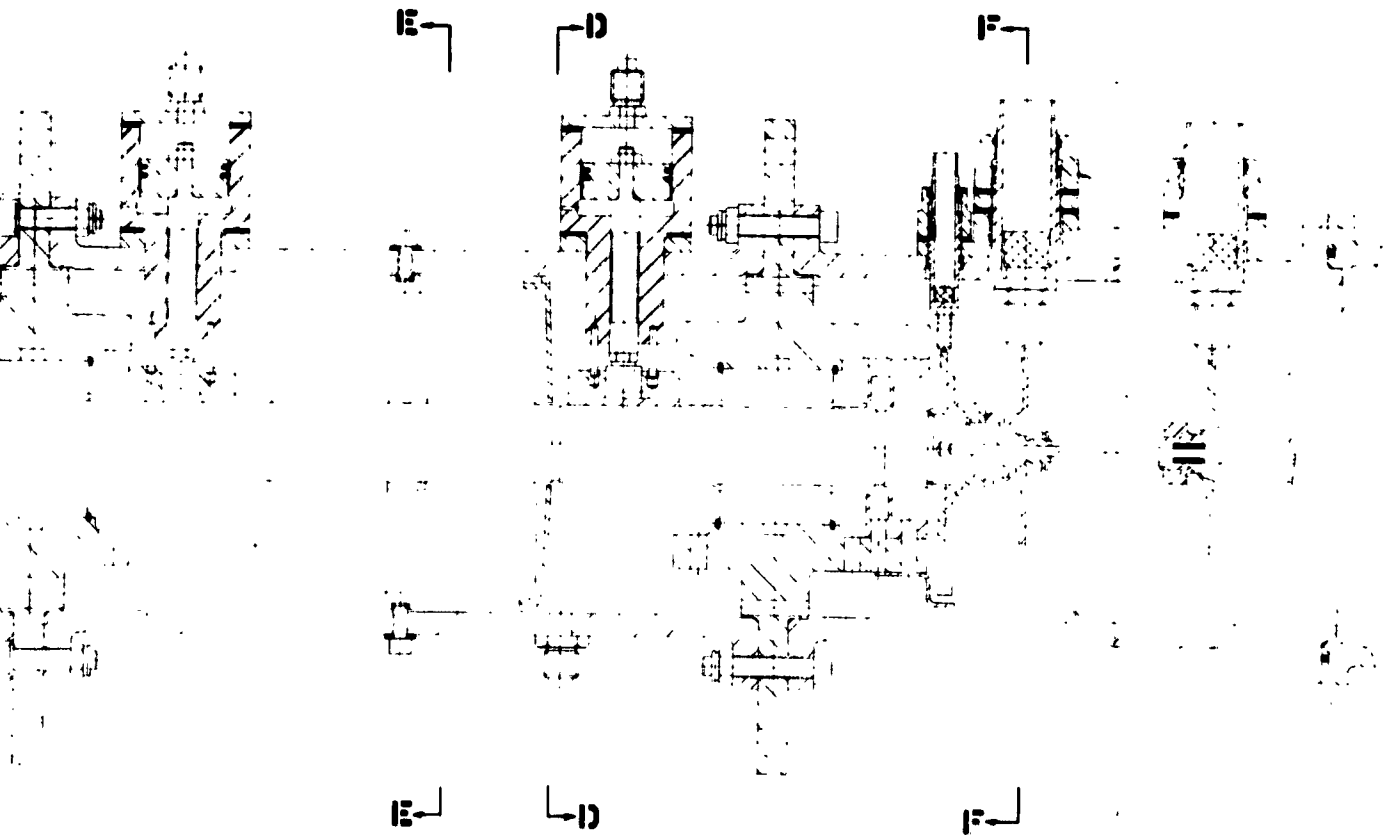

Figure

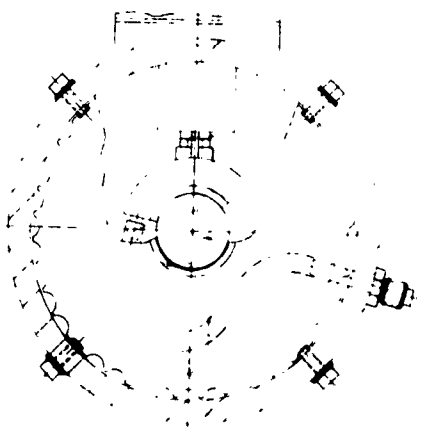

SECT E-E

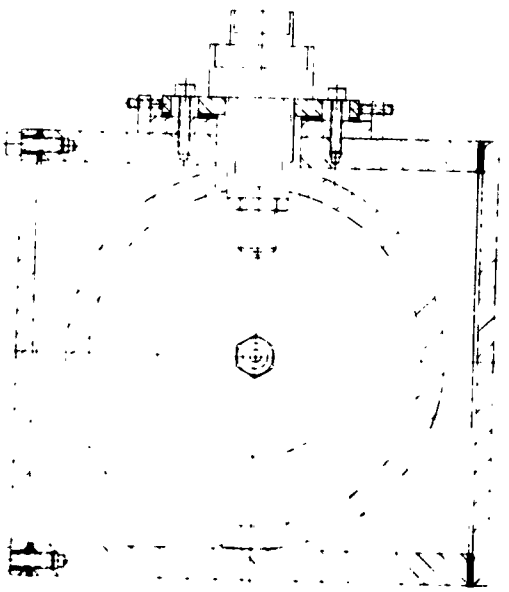

SECT F-F

3

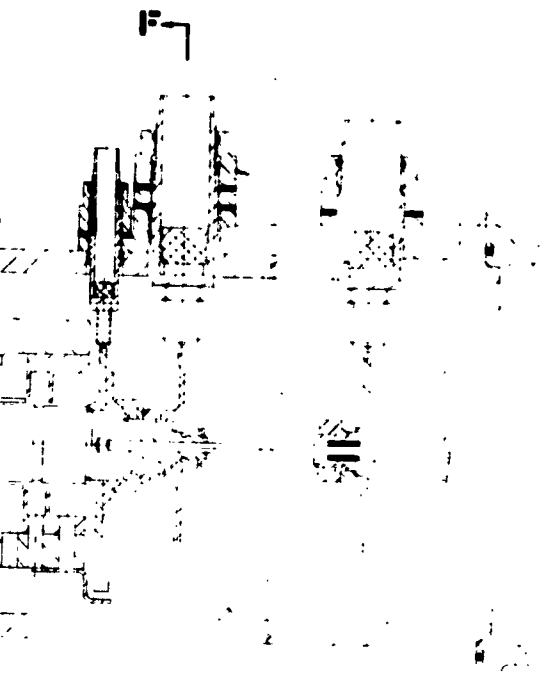

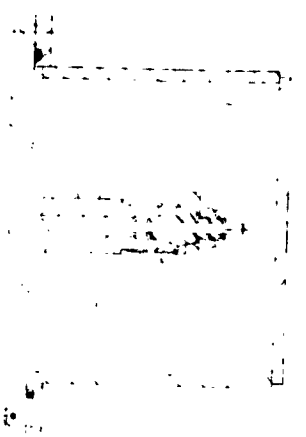

Figure 4. Bearing Stability Test Rig Assembly
Shaft Diameter - D = 1.25

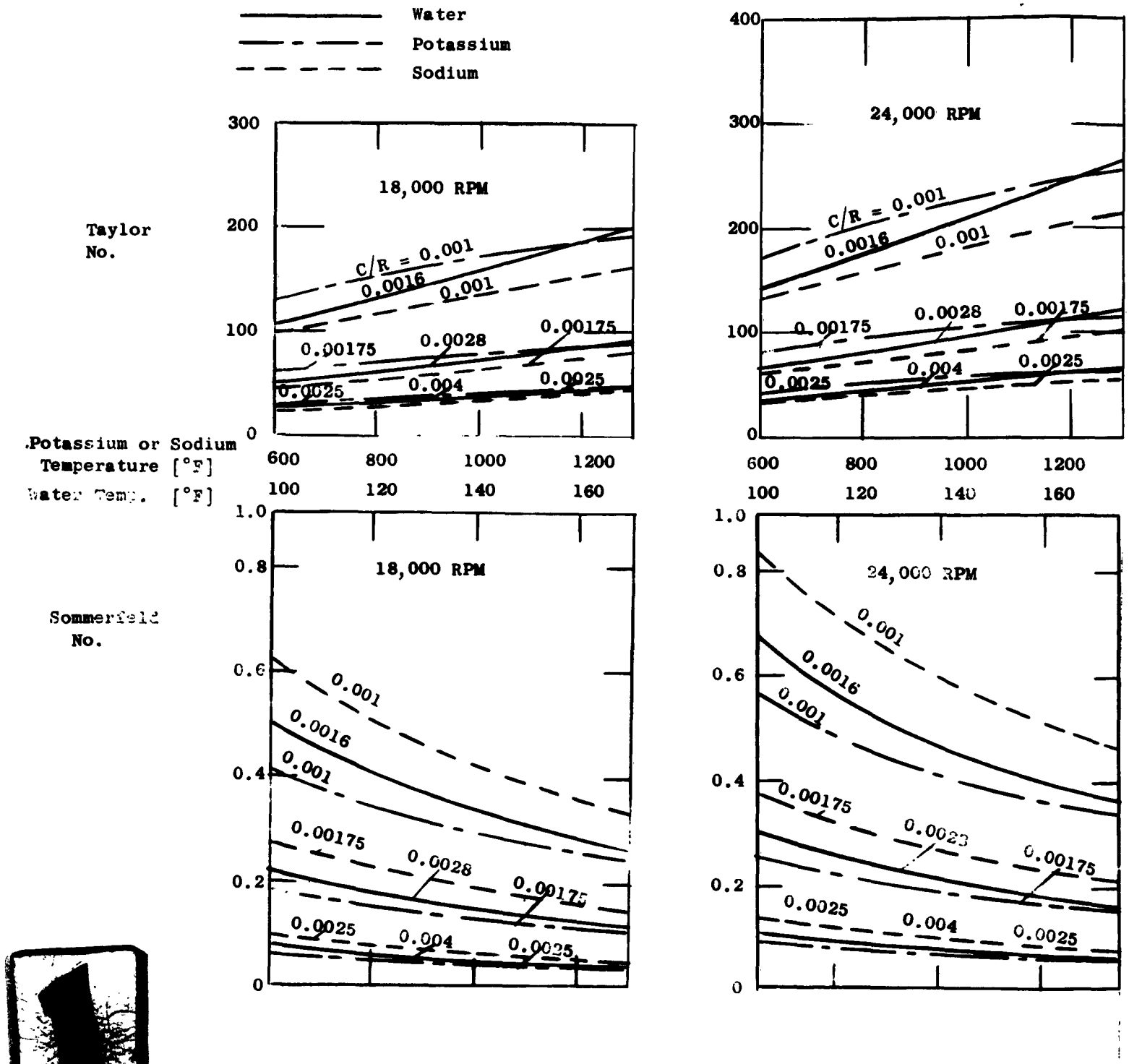

Figure .. Clearance Selection for Test Bearings.

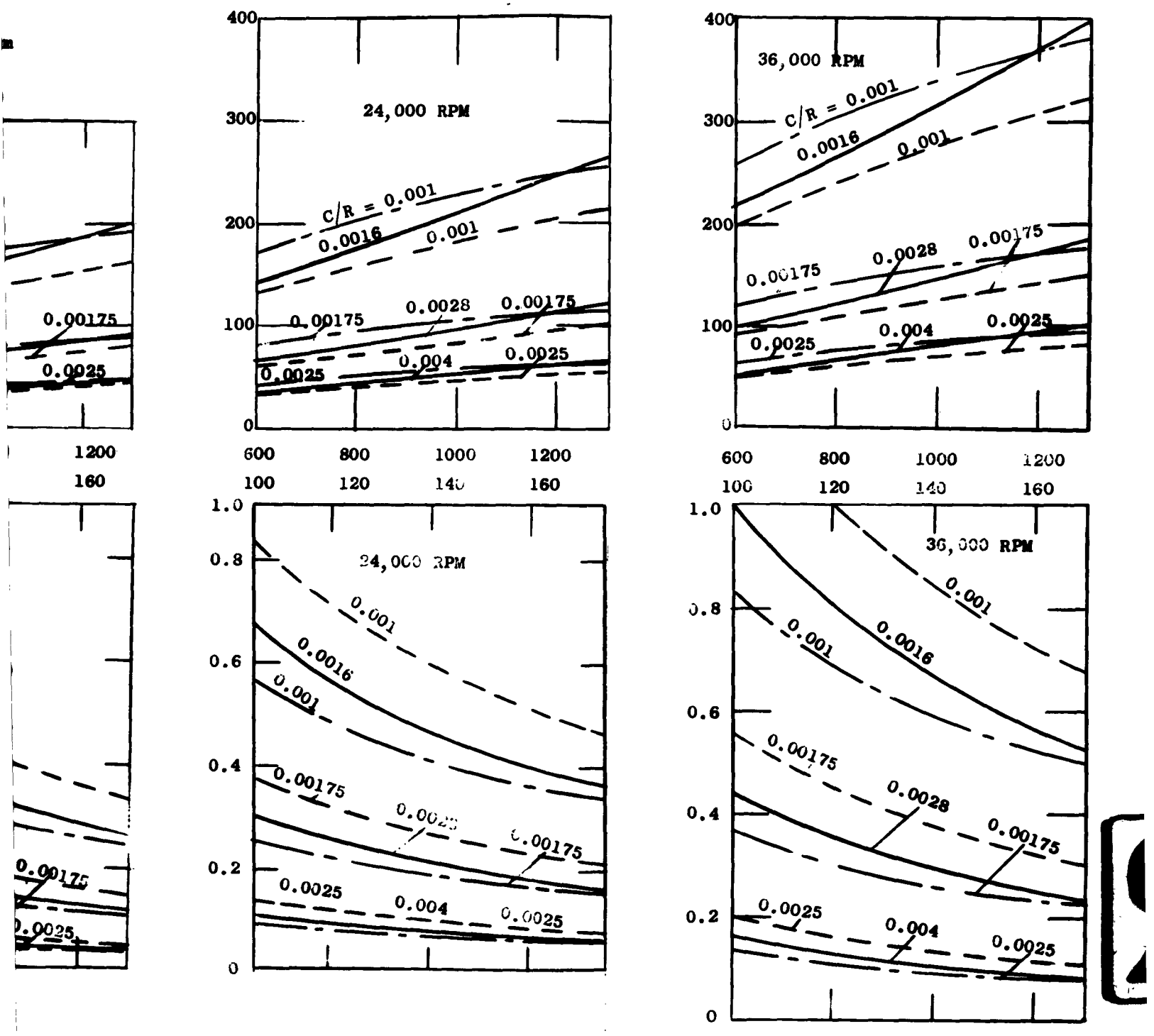

Figure 5. Clearance Selection for Test Bearings.

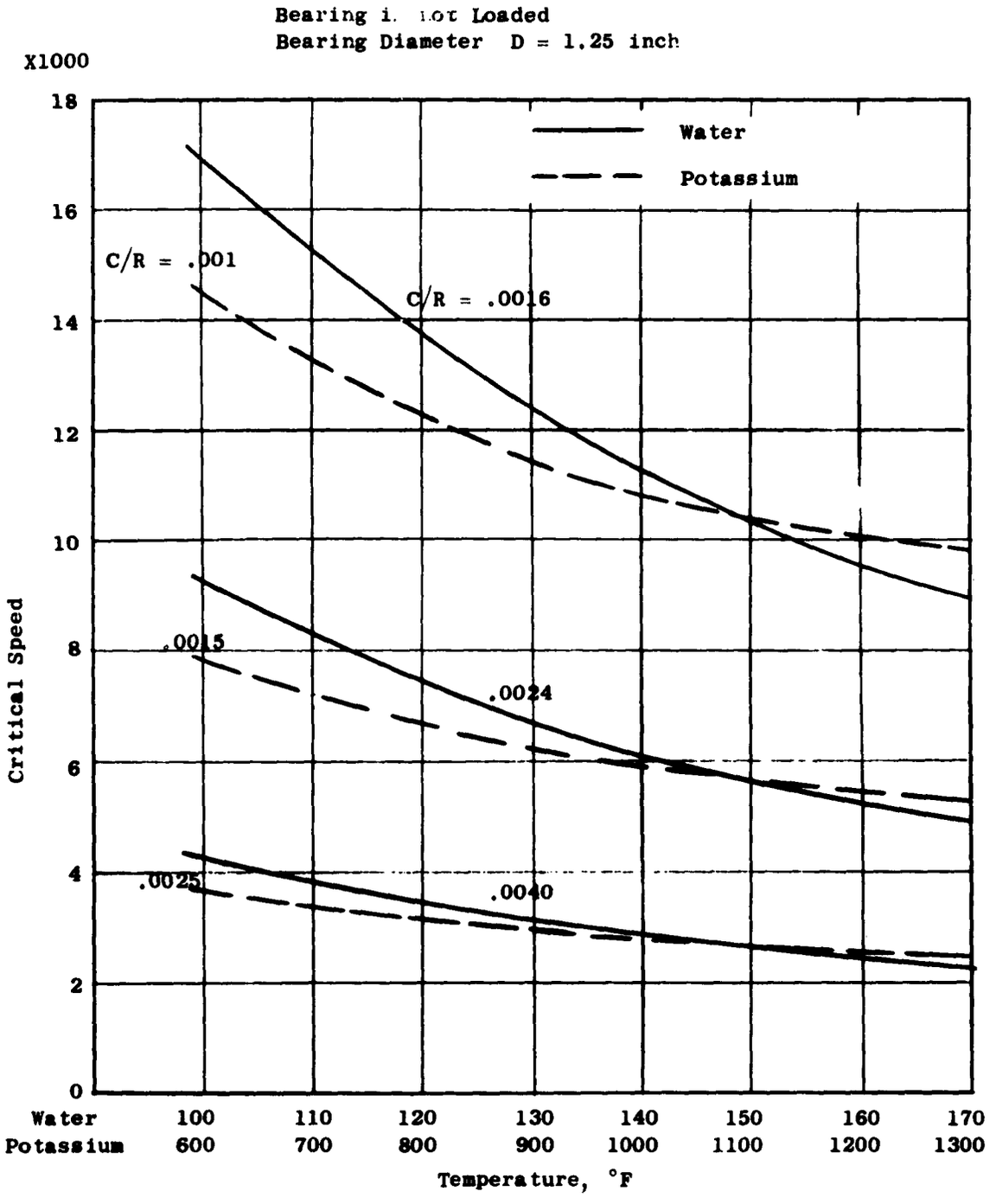

Figure 6. Transition Speed from Laminar to Turbulent Bearing Operation as a Function of Lubricant Temperature

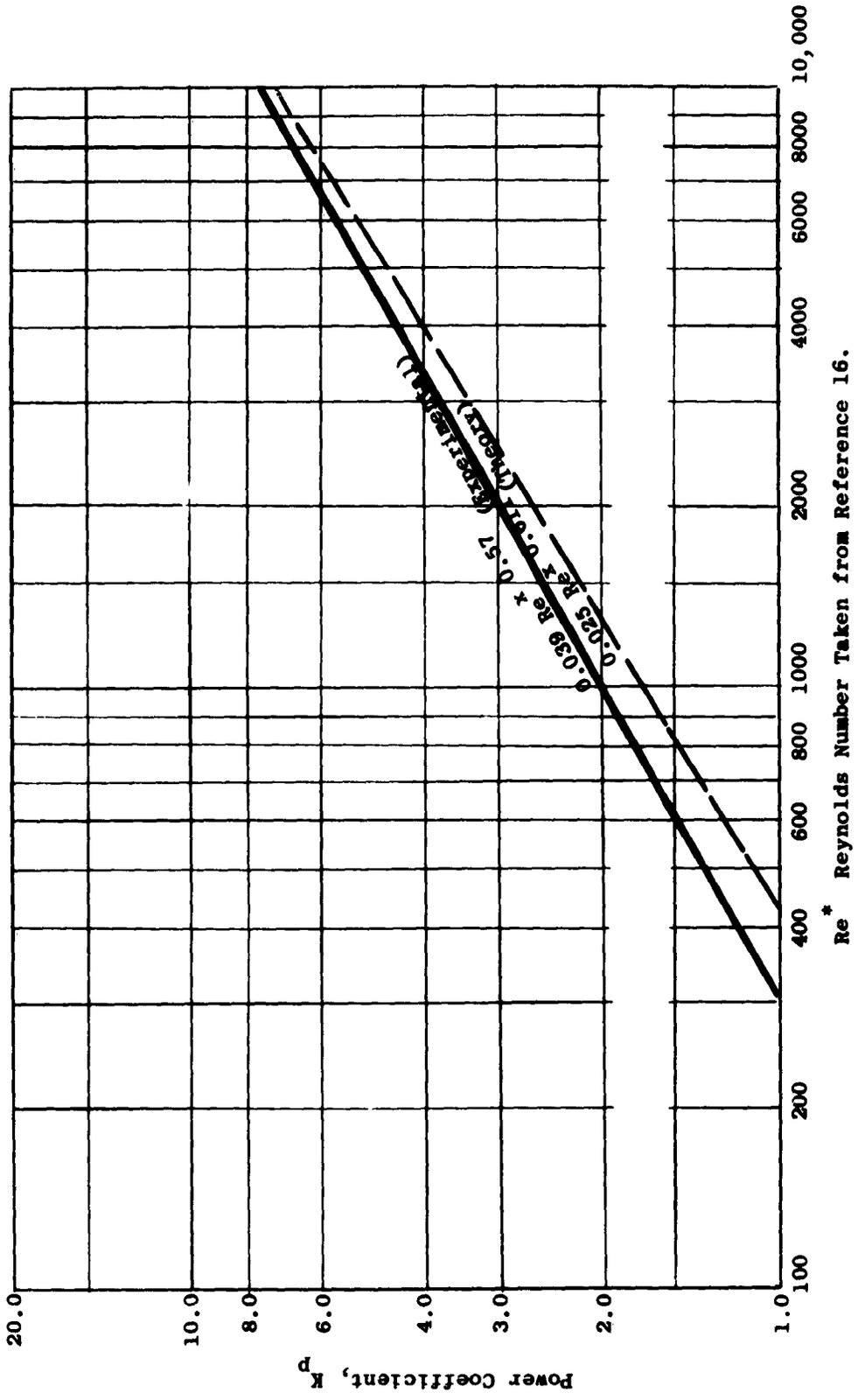

Figure 7. Power Coefficient K_p v. Reynolds Number for Journal Bearings.

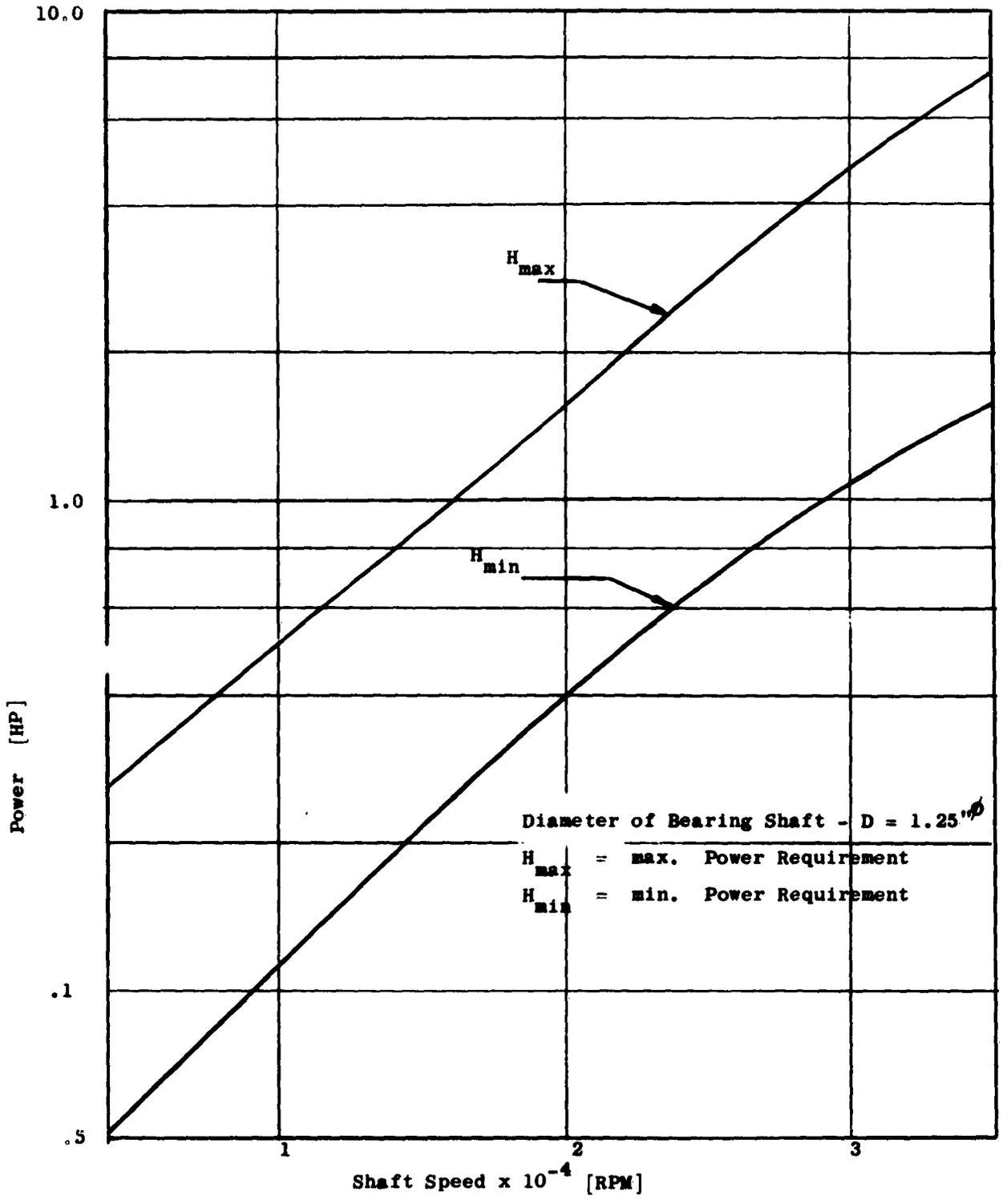

Figure 8. Power Which Has to be Transmitted by the Quill Shaft vs. Shaft Speed.

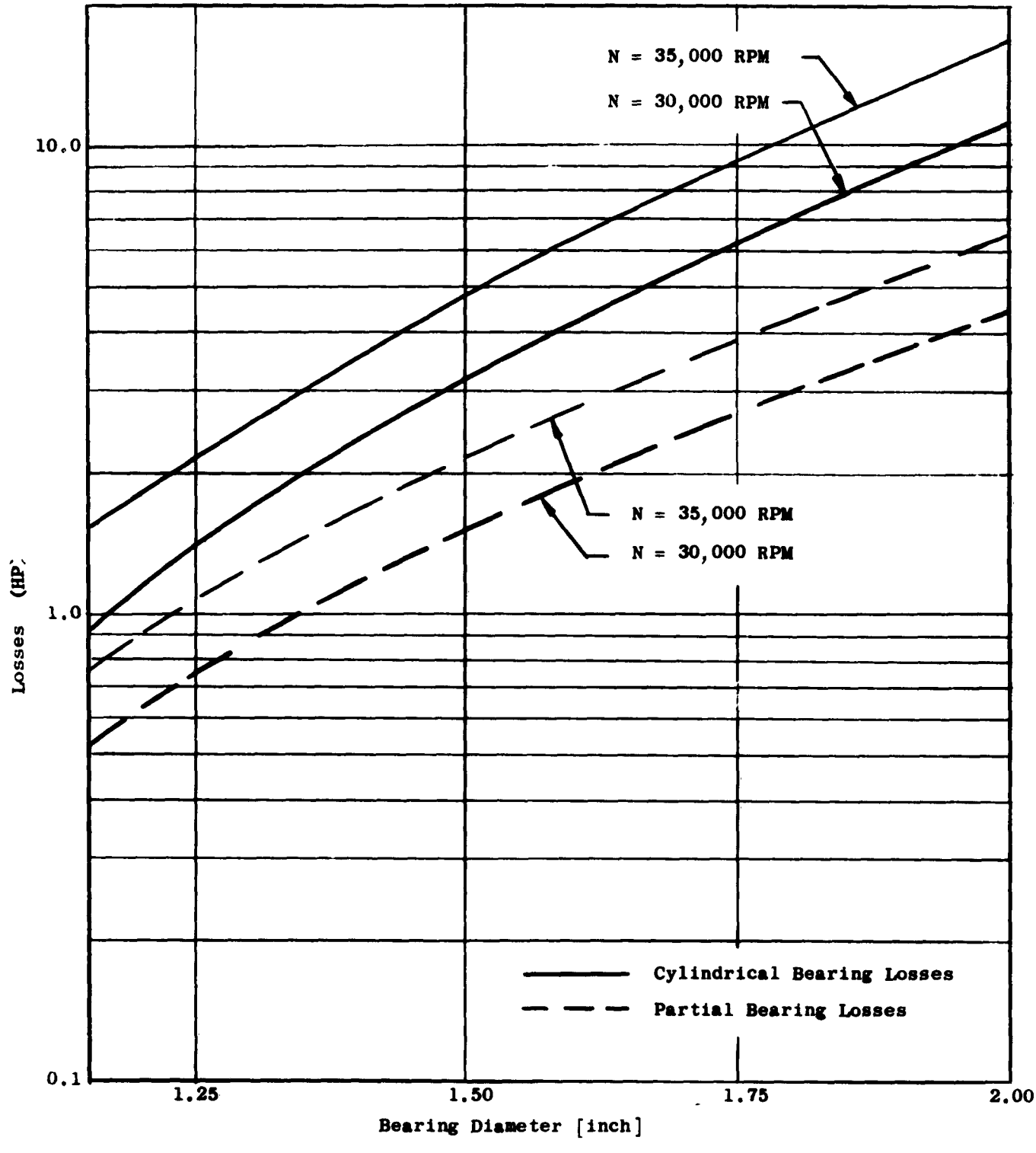

Figure 9. Bearing Losses/Bearing vs. Bearing Diameter.

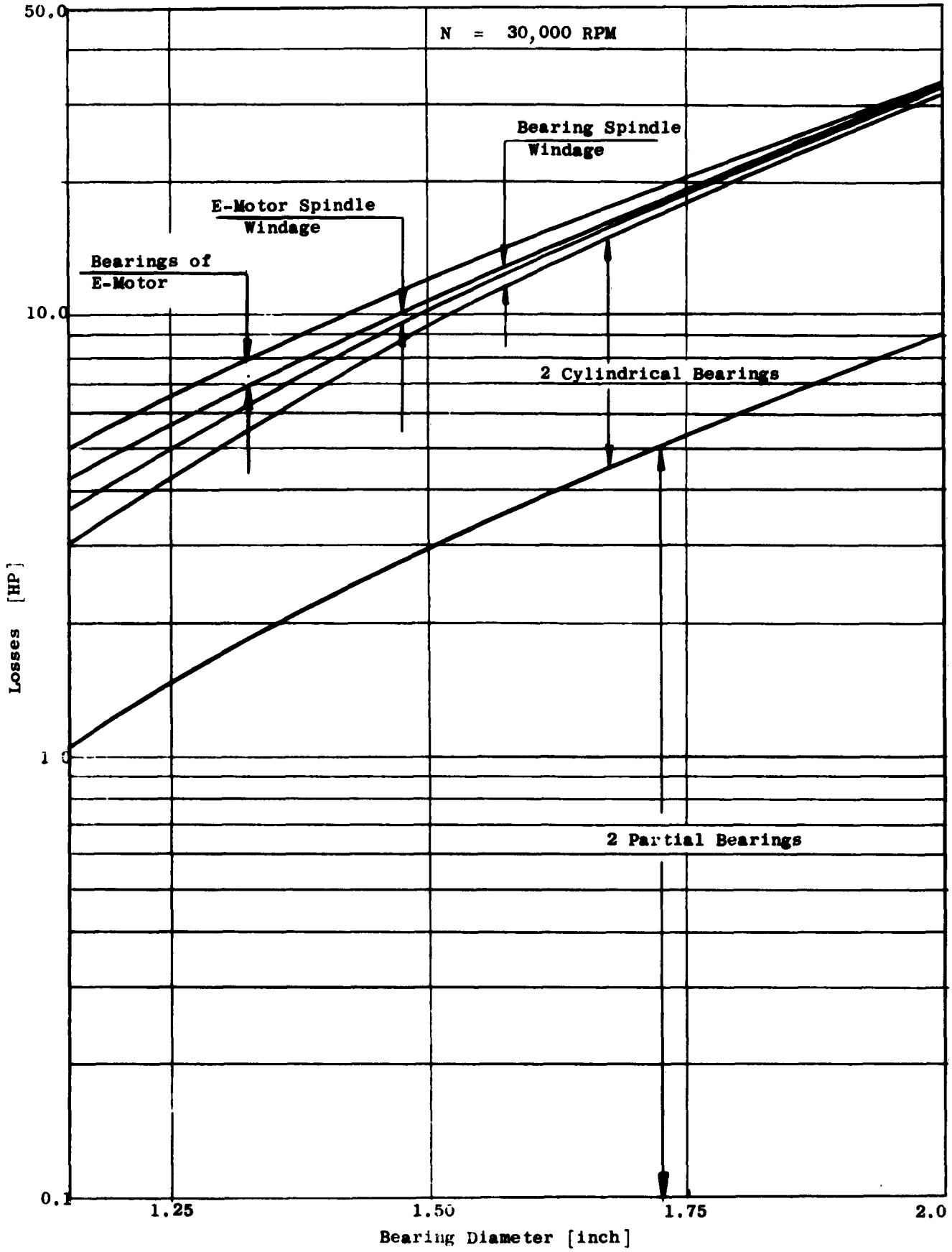

Figure 10. Power Requirements of Bearing Stability Test Rig vs. Bearing Diameter.

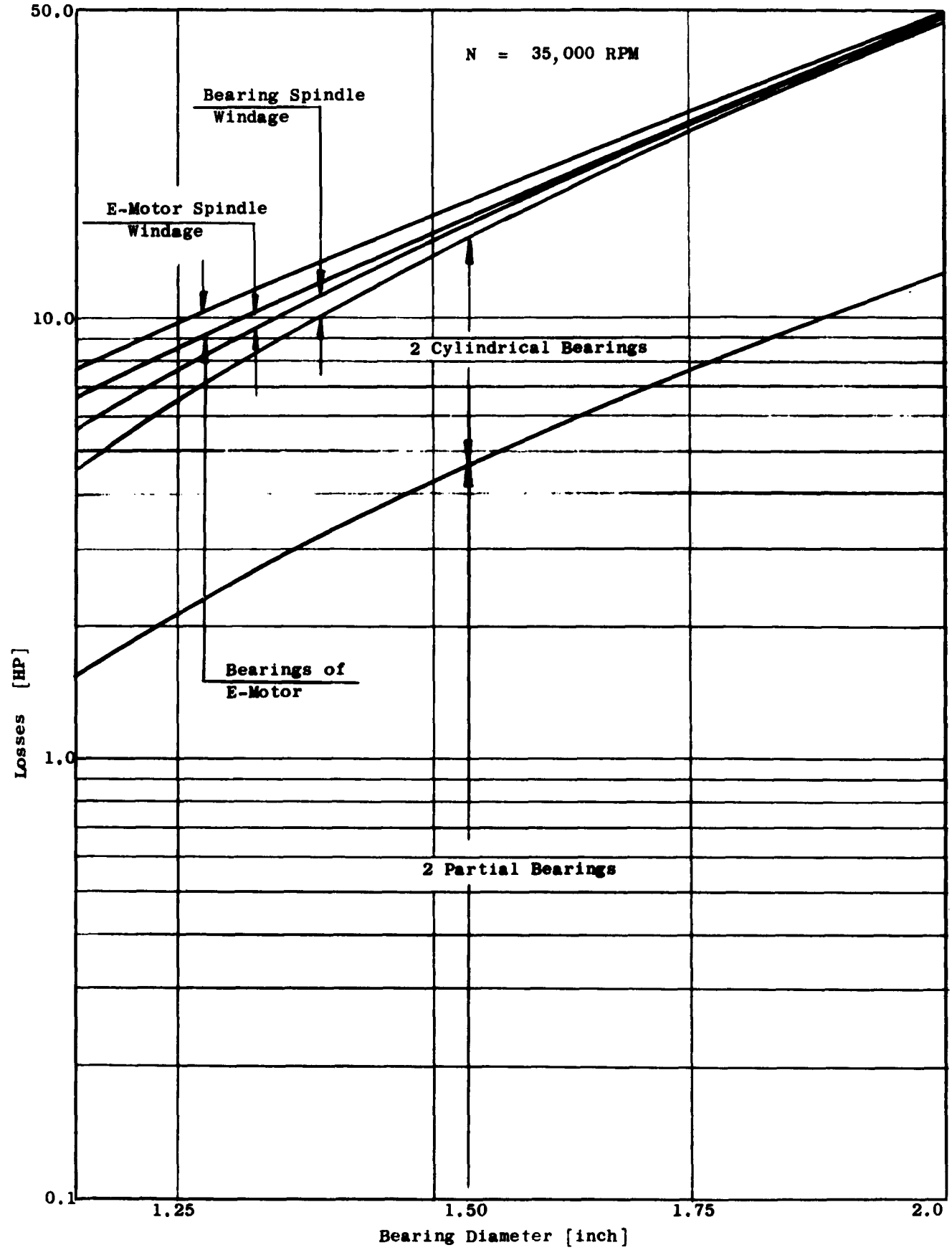

Figure 11. Power Requirements of Bearing Stability Test Rig vs. Bearing Diameter.

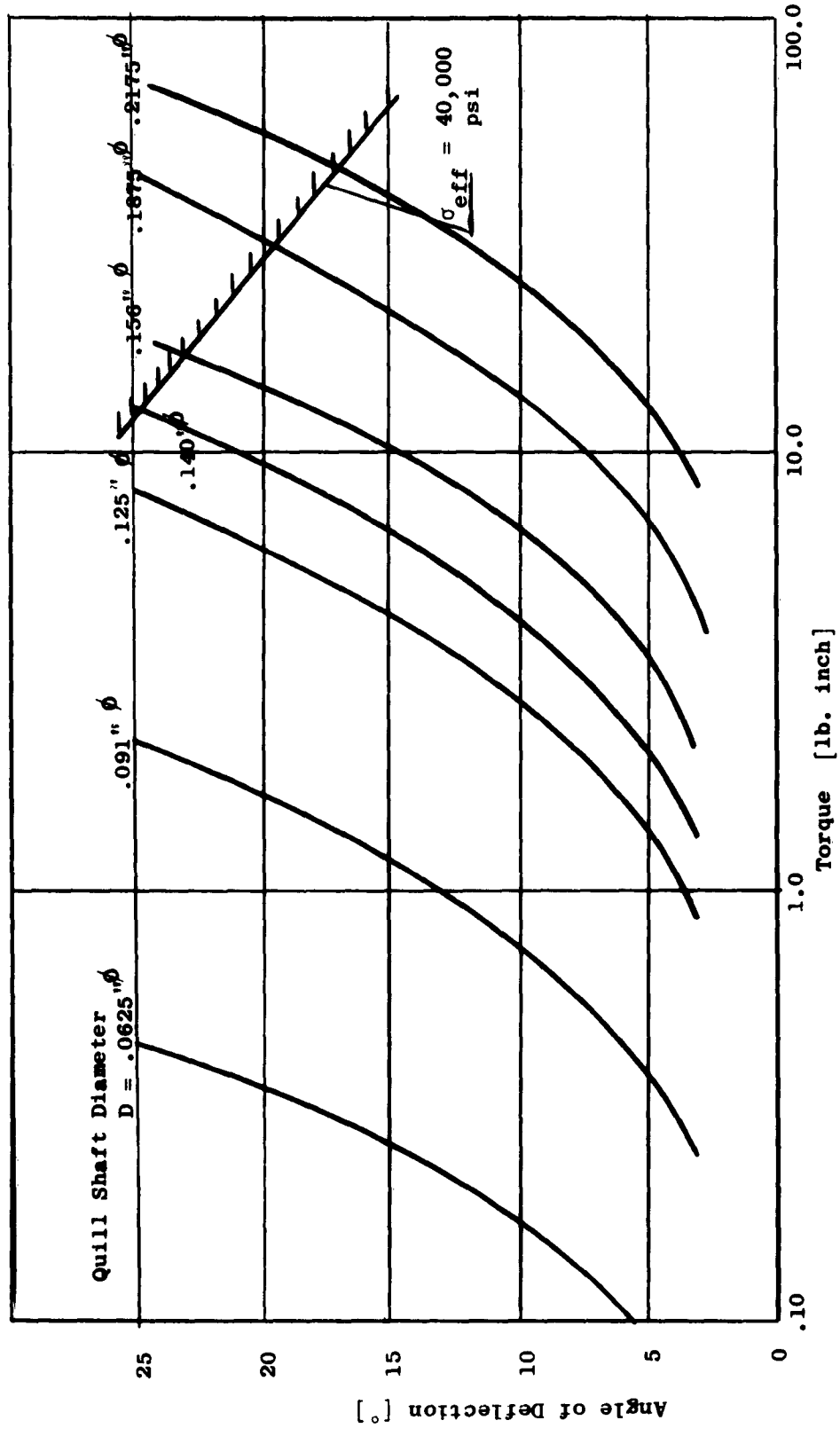

Figure 12. Angular Deflection of Quill Shaft as Function of Transmitted Torque.

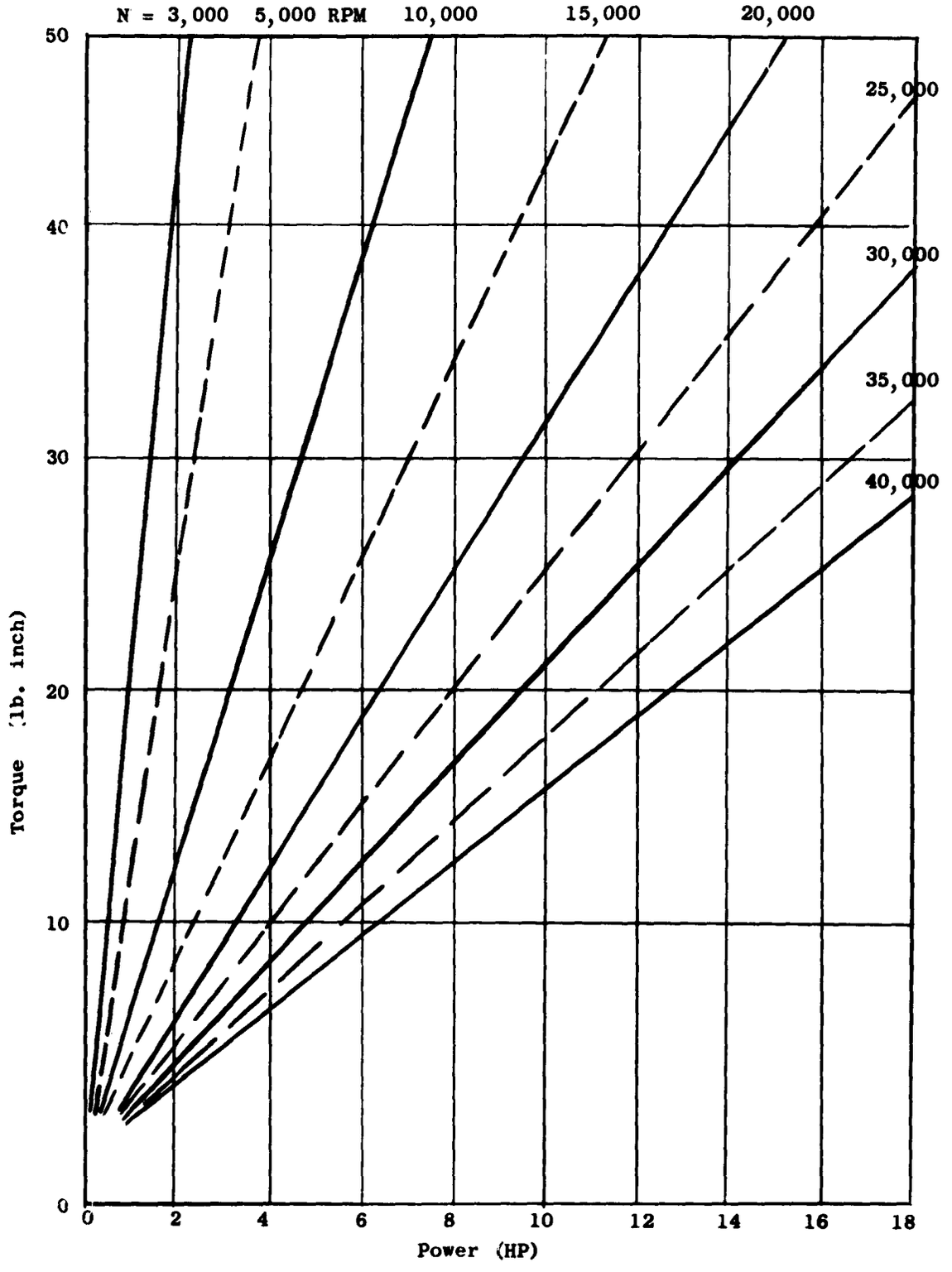

Figure 13. Torque vs. Power

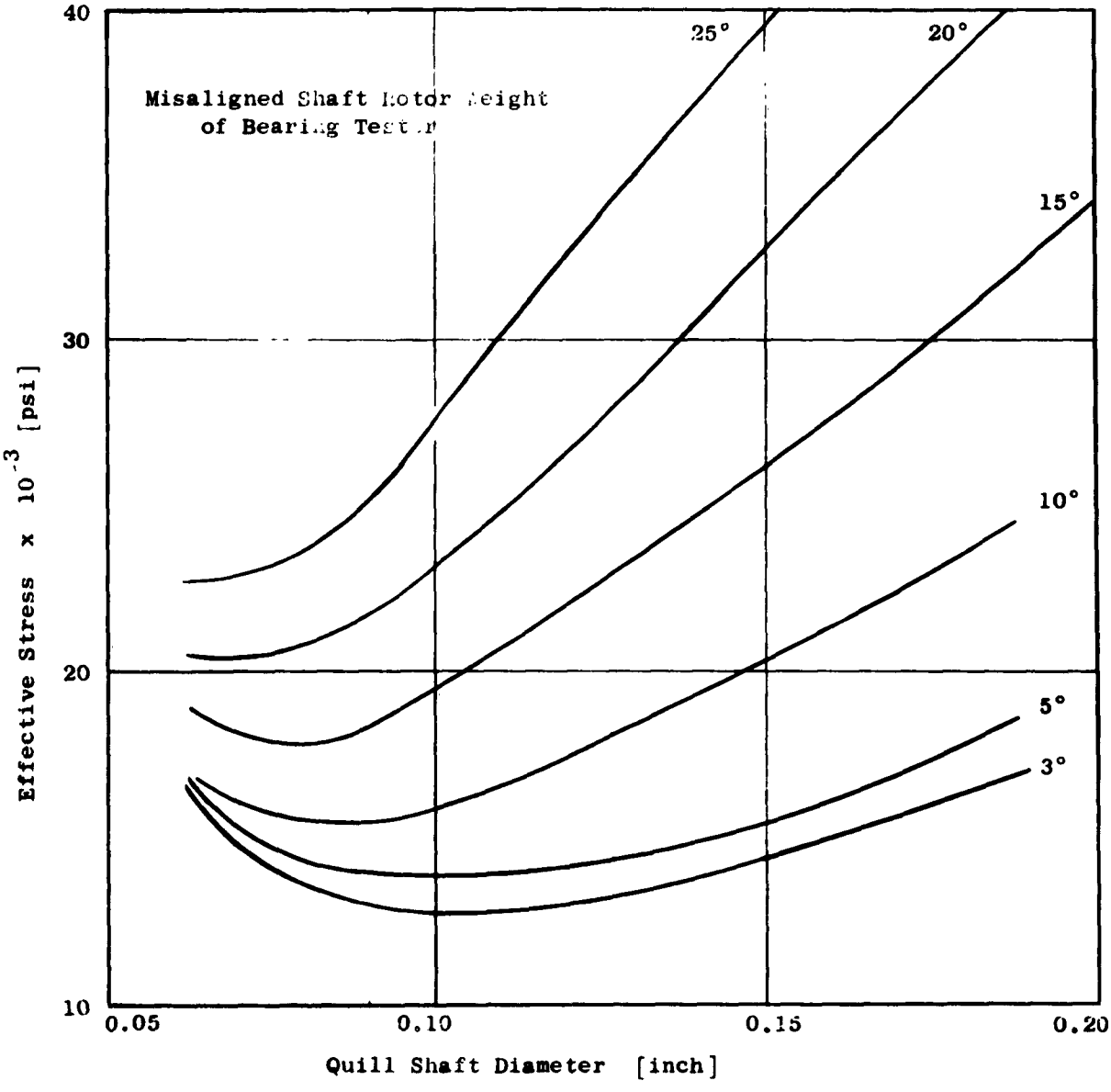

Figure 14. Quill Shaft Stresses vs. Shaft Diameter

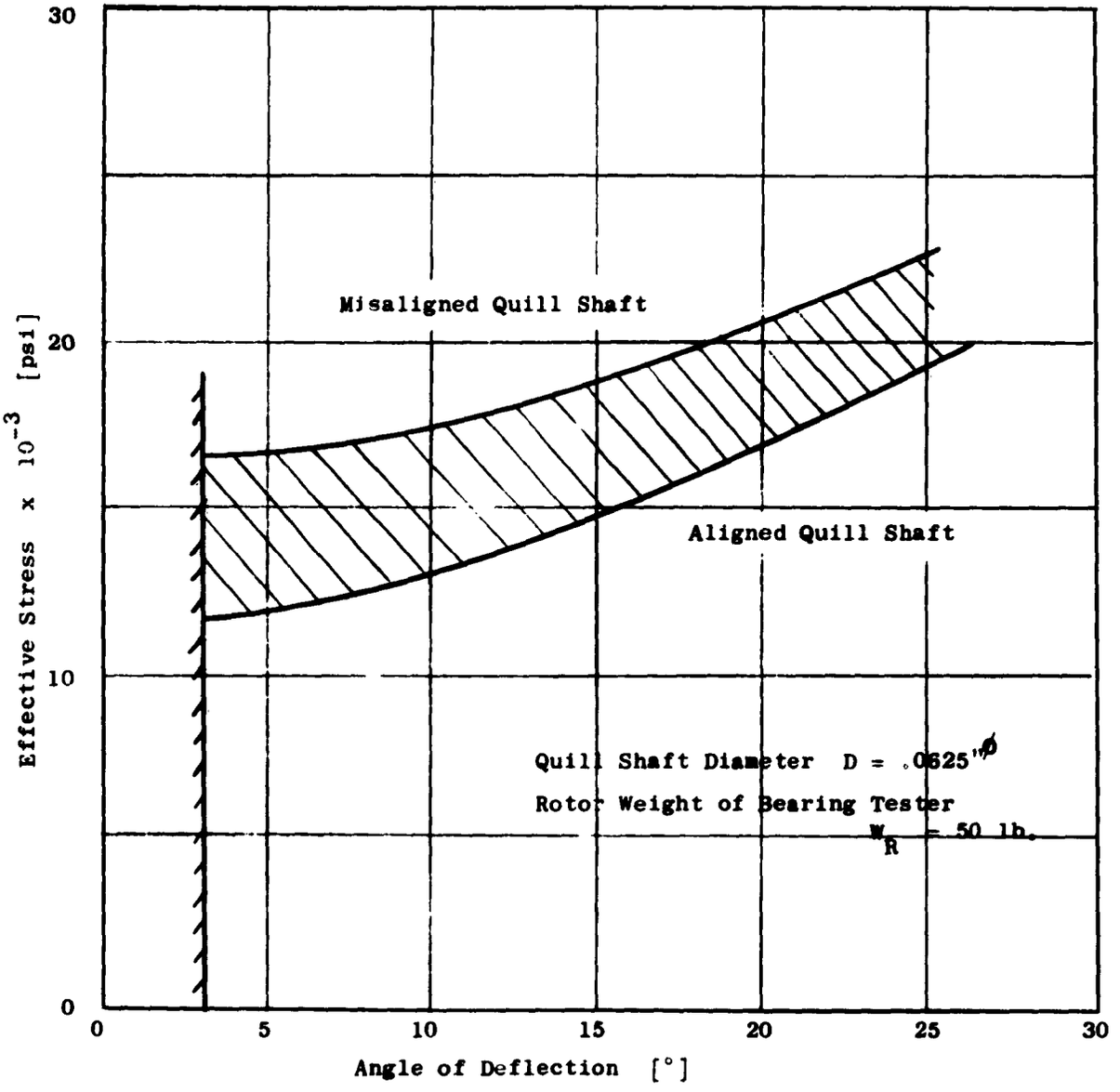

Figure 15. Quill Shaft Stresses vs. Angular Deflection.

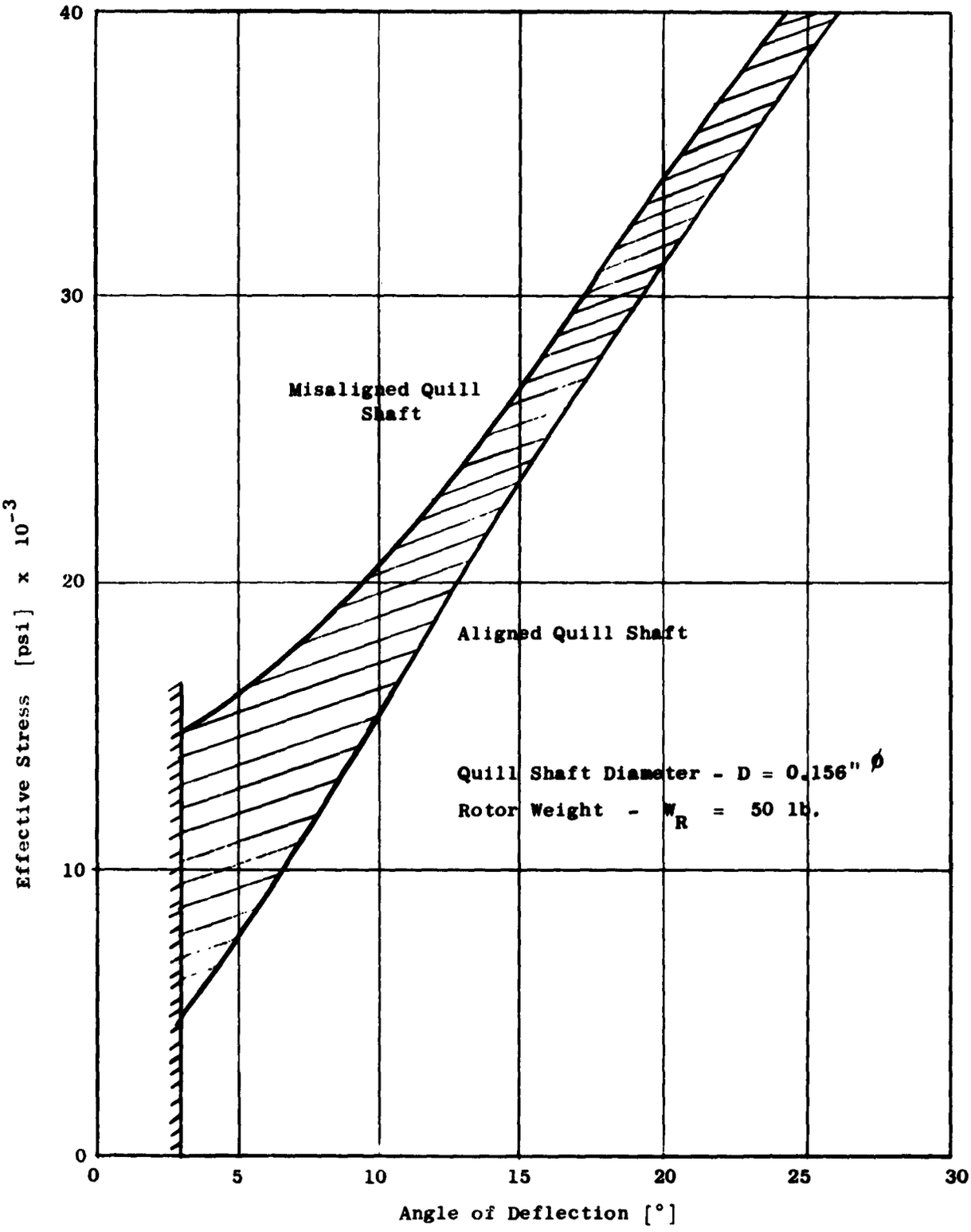

Figure 16. Quill Shaft Stresses vs. Angular Deflection.

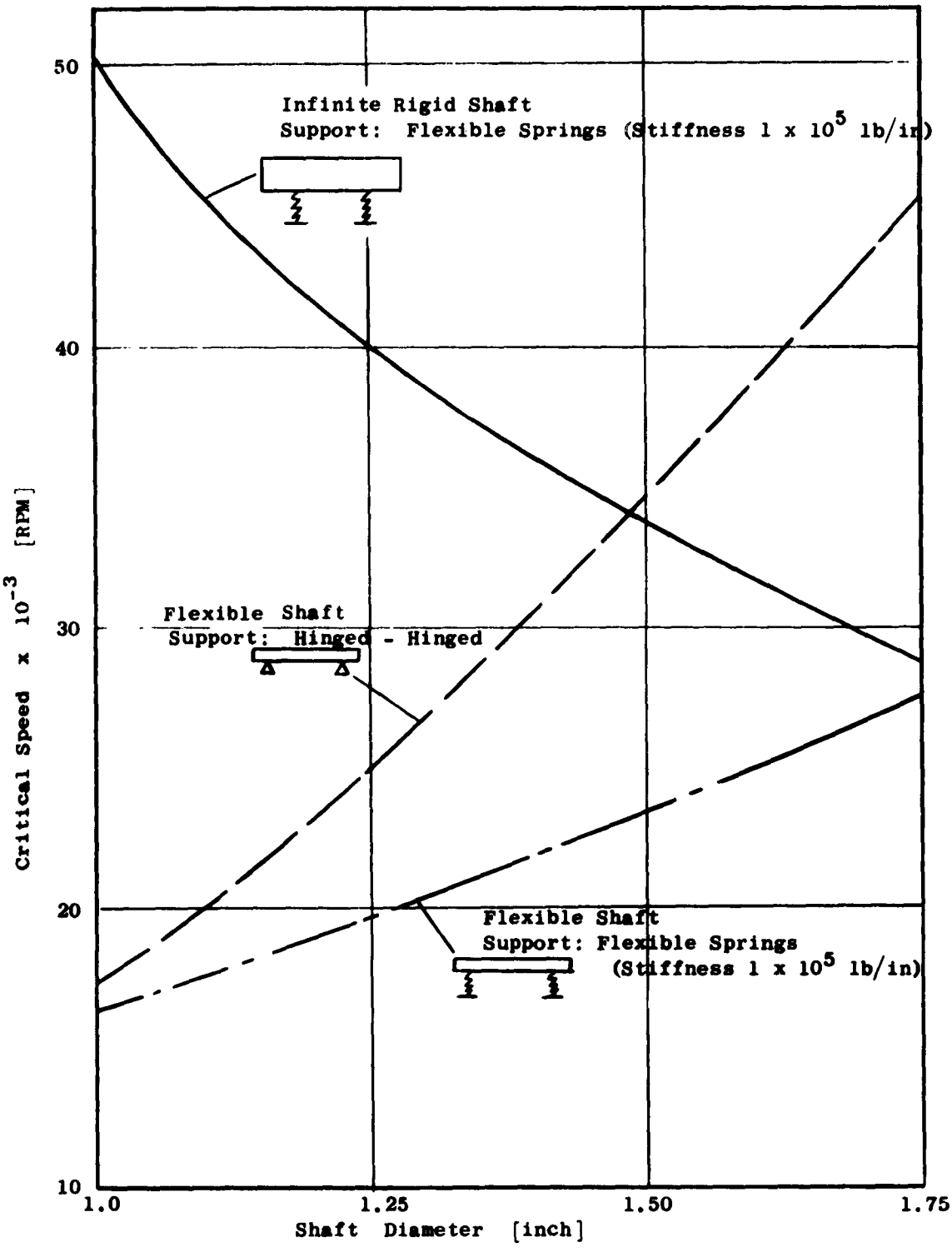

Figure 17. Critical Shaft Speed vs. Shaft Diameter.

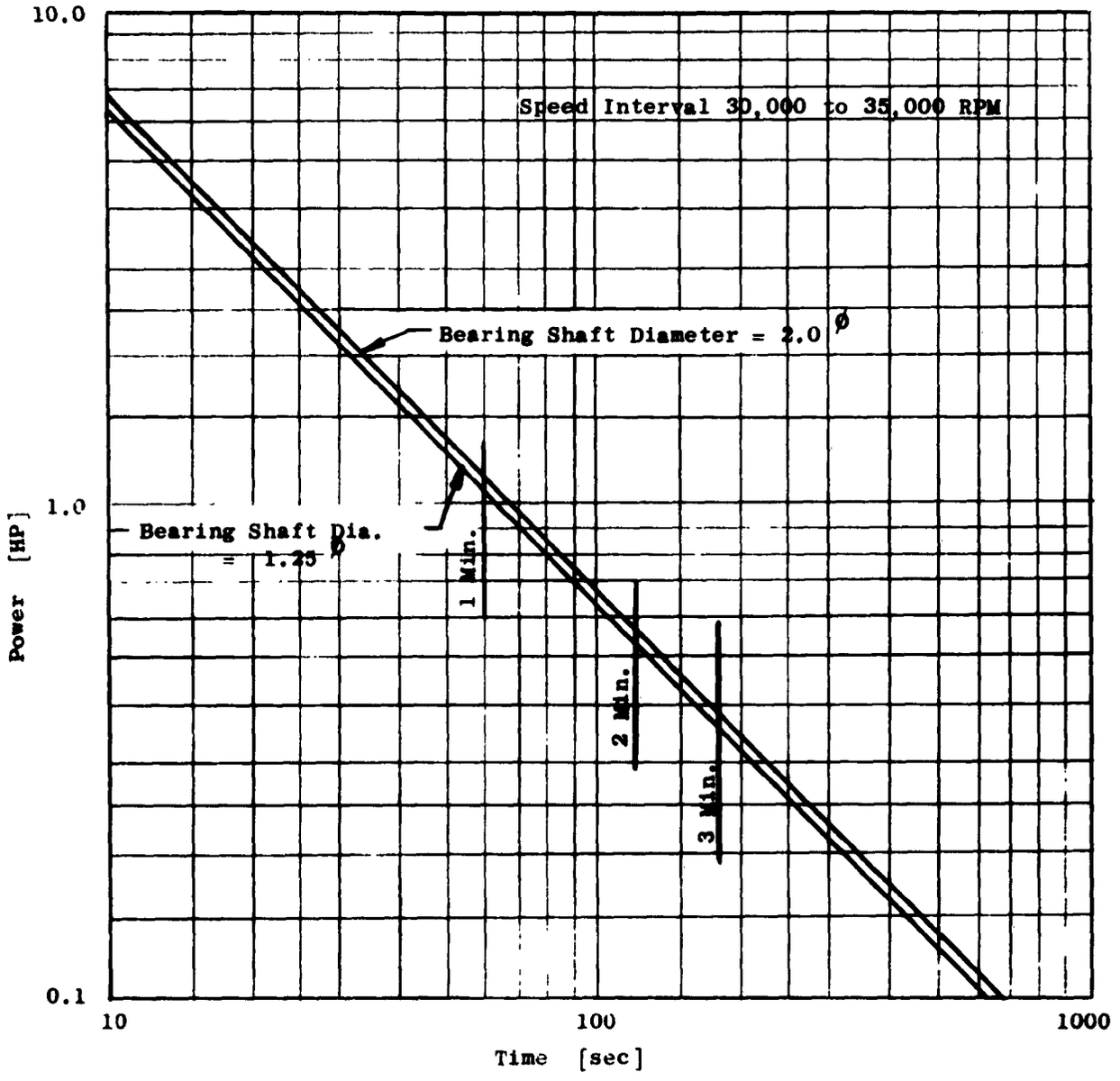

Figure 19. Power Requirements for Accelleration of Test Rig Shafts vs. Time.

Figure 20. Bearing Stability Program Schedule

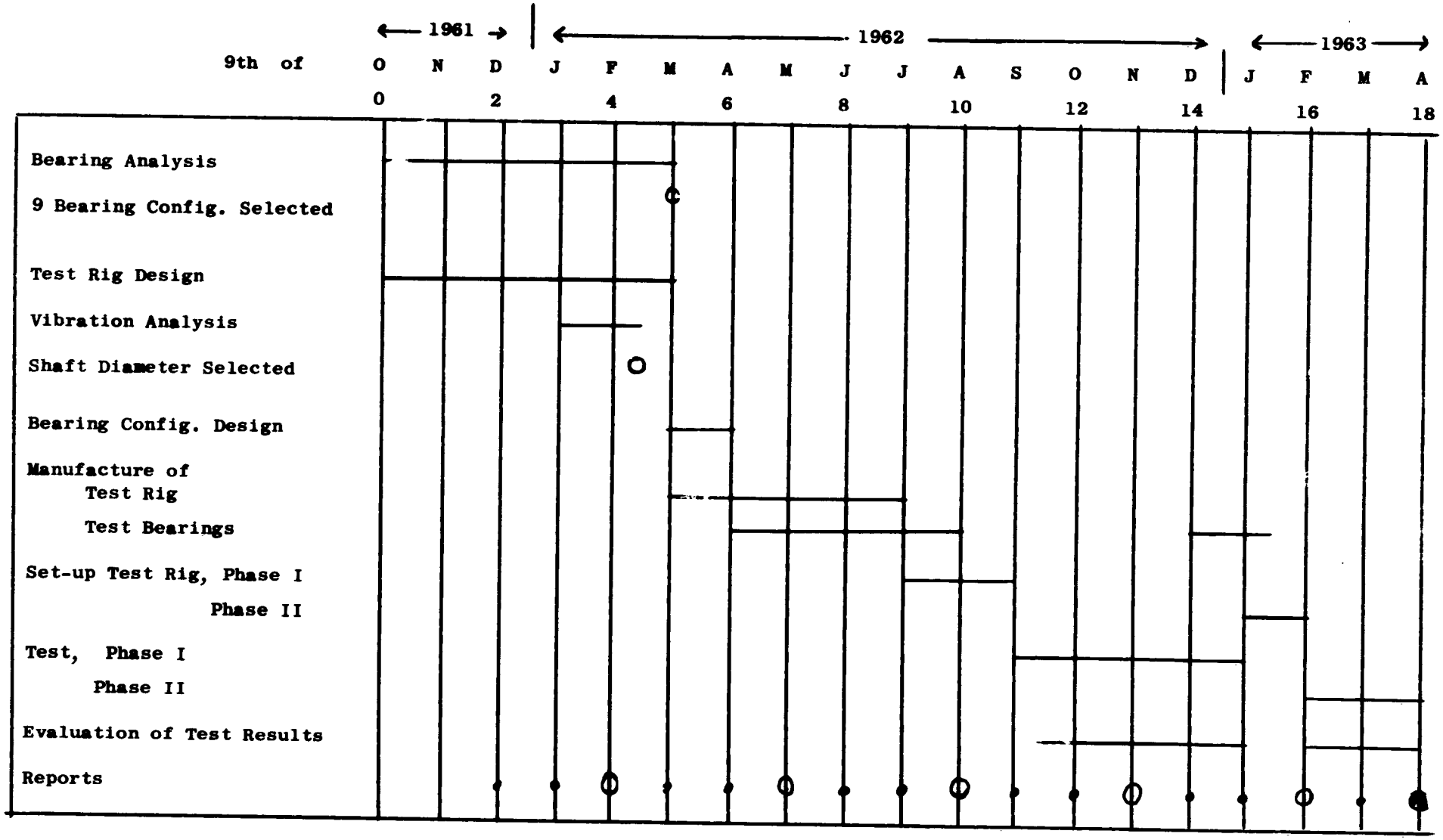

DISTRIBUTION LIST

Advanced Research Project Agency
The Pentagon
Washington 25, D. C.
ATTN: Mr. John Huth

Air University Library
Maxwell Air Force Base, Alabama
ATTN: Director

ASTIA
Fort Myer, Virginia

Armour Research Foundation of Illinois
Institute of Technology
Technology Center
Chicago 16, Illinois
ATTN: Dr. W. H. Baier

Aerojet-General Corporation
Power/Equipment Division
Azusa, California
ATTN: Mr. A. M. Taylor

Allison Division
General Motors Corporation
Indianapolis, Indiana
ATTN: Mr. D. T. Lawrence

Atomics International
P. O. Box 309
Canoga Park, California
ATTN: Mr. Carl E. Johnson

Battelle Memorial Institute
505 King Avenue
Columbus 1, Ohio
ATTN: Dr. R. W. Dayton

E. I. du Pont de Nemours & Co., Inc.
Development Department
Wilmington, Delaware
ATTN: Mr. E. H. Schmidt

The Garrett Corporation
AiResearch Manufacturing Division
Phoenix, Arizona
ATTN: Mr. E. S. Cain

General Electric Company
Missile & Space Vehicle Dept.
3198 Chestnut Street
Philadelphia 4, Pennsylvania
ATTN: Mr. Edward Ray
Space Power Project

General Atomic Division
P. O. Box 8, Oldtown Station
San Diego 10, California
ATTN: Mr. R. W. Pidd

Materials Central
Fluids & Lubricants Branch
Wright-Patterson Air Force Base, Ohio
ATTN: Mr. R. J. Benzing
Fluids & Films Section

MSA Research Corporation
Callery, Pennsylvania
ATTN: Mr. G. E. Kennedy

National Aeronautics & Space Administration
1520 H Street, N. W.
Washington 25, D. C.
ATTN: Dr. Fred Schulman (RN)
Program Director

National Aeronautics & Space Administration
Lewis Research Center
21000 Brookpark Road
Cleveland 35, Ohio
ATTN: Henry O. Slone (2 plus repro.)
Space Electric Power Office

National Aeronautics & Space Administration
Lewis Research Center
21000 Brookpark Road
Cleveland 35, Ohio
ATTN: Mr. Robert E. English
Nuclear Systems Division

National Aeronautics & Space Administration
Lewis Research Center
21000 Brookpark Road
Cleveland 35, Ohio
ATTN: Mr. Warner L. Stewart
Fluid System Components Division

National Aeronautics & Space Administration
Lewis Research Center
21000 Brookpark Road
Cleveland 35, Ohio
ATTN: Mr. James H. Dunn

National Aeronautics and Space Administration
Jet Propulsion Laboratory
California Institute of Technology
4800 Oak Grove Drive
Pasadena, California
ATTN: Mr. John Paulson

National Aeronautics and Space Administration
Lewis Research Center
21000 Brookpark Road
Cleveland 35, Ohio
ATTN: Mr. William J. Anderson
Fluid Systems Components Division

National Aeronautics & Space Administration
Lewis Research Center
21000 Brookpark Road
Cleveland 35, Ohio
ATTN: Mr. Thomas P. Moffitt
Fluid Systems Components Division

National Aeronautics & Space Administration
Lewis Research Center
21000 Brookpark Road
Cleveland 35, Ohio
ATTN: Mr. Joseph P. Joyce
Space Electric Power Office

National Aeronautics & Space Administration
Lewis Research Center
21000 Brookpark Road
Cleveland 35, Ohio
ATTN: Mr. Robert L. Johnson
Fluid Systems Components Division

National Aeronautics & Space Administration
Lewis Research Center
21000 Brookpark Road
Cleveland 35, Ohio
ATTN: Mr. George Mandel
Library

National Aeronautics & Space Administration
Goddard Space Flight Center
Greenbelt, Maryland
ATTN: Office of Technical Information
Code 250

National Aeronautics & Space Administration
Western Operations Office
150 Pico Boulevard
Santa Monica, California
ATTN: Mr. John Keeler

National Aeronautics & Space Administration
Lewis Research Center
21000 Brookpark Road
Cleveland 35, Ohio
ATTN: Mr. John R. Biggs
Procurement & Supply Division

Pratt & Whitney Aircraft
Division of United Aircraft Corp.
East Hartford, Connecticut
ATTN: Mr. R. P. Shevchenko

The RAND Corporation
1700 Main Street
Santa Monica, California
ATTN: Mr. F. R. Collbohm

Rocketdyne
Nucleonics Subdivision
Rocketdyne Engineering
Canoga Park, California
ATTN: Mr. R. B. Dillaway

Sundstrand Aviation-Denver
A Division of Sundstrand Corporation
Denver 21, Colorado
ATTN: Mr. P. H. Stahlhuth

Southwest Research Institute
8500 Culebra Road
San Antonio 6, Texas
ATTN: Dr. R. A. Burton

TAPCO
A Division of Thompson Ramo Wooldridge
New Devices Laboratories
Cleveland 4, Ohio
ATTN: Mr. D. C. Reemsnyder

U. S. Atomic Energy Commission
Technical Information Service Extension
P. O. Box 62
Oak Ridge, Tennessee

Westinghouse Electric Corporation
Research Laboratories
Pittsburgh, Pennsylvania
ATTN: Mr. J. Boyd

Air Force Systems Command
Aeronautical Systems Division
Wright-Patterson Air Force Base, Ohio
ATTN: Mr. Bernard Chasman - ASRCE

Air Force Systems Command
Aeronautical Systems Division
Wright-Patterson Air Force Base, Ohio
ATTN: Mr. J. L. Morris - ASRCNL-2

Oak Ridge National Laboratory
P. O. Box Y
Oak Ridge, Tennessee
ATTN: Mr. H. W. Savage